

***Geoinformation Issues***  
*Problemy geoinformacji*

**2015**  
**Vol. 7 No 1 (7)**



# GEOINFORMATION ISSUES

## PROBLEMY GEOINFORMACJI

In the journal there are printed peer-reviewed articles containing the results of research on theoretical, experimental and applicable problems in the field of geodesy, surveying engineering, photogrammetry, cartography, GIS and remote sensing

### EDITORIAL BOARD

#### **Editor-in-Chief**

Jan Kryński

#### **Executive members**

Marek Baranowski, Robert Wł. Bauer (Chairman), Aleksander Brzeziński, Katarzyna Dąbrowska-Zielińska, Dariusz Gotlib, Jan Kryński, Jan R. Olędzki

#### **Foreign members**

Rene Forsberg (Denmark), Georg Gartner (Austria), Jan Hefty (Slovakia), Aleksander Kent (UK), Eimuntas Parseliunas (Lithuania), Petter Pilesjo (Sweden), Rostyslav Sossa (Ukraine), Gregory Taff (Norway)

#### **Technical secretary**

Teresa Konarska

#### **Technical editor**

Paulina Waszkiewicz

#### **Cover designer**

Marek Baranowski

### EDITOR'S OFFICE

Institute of Geodesy and Cartography

27 Modzelewskiego St.

02-679 Warsaw, Poland

Tel.: +48 22 3291918, Fax: +48 22 3291950

www: [igik.edu.pl](http://igik.edu.pl), e-mail: [boi@igik.edu.pl](mailto:boi@igik.edu.pl)

© Institute of Geodesy and Cartography

ISSN 1689-6440

IGiK, Warsaw 2015

Hard copy of the journal is its primary version

## Contents

### Spis treści

Walyeldeen Godah

Malgorzata Szelachowska

Jan Krynski

**On the selection of GRACE-based GGMs and a filtering method for estimating mass variations in the Earth system over Poland** ..... 5

Wybór globalnych modeli geopotencjału opracowanych na podstawie danych z misji GRACE oraz metody filtracji, do wyznaczania zmian rozkładu mas w systemie Ziemia na obszarze Polski

Michał Kruczyk

**Comparison of techniques for Integrated Precipitable Water measurement in the polar region** ..... 15

Porównanie technik pomiarów kolumnowej zawartości pary wodnej w obszarze polarnym

Zbigniew Bochenek

Dariusz Ziółkowski

Maciej Bartold

**Application of NOAA AVHRR satellite images for studying various environmental and climatic conditions in Polish forests** ..... 29

Zastosowanie obrazów satelitarnych NOAA AVHRR do badania warunków środowiskowych i klimatycznych w polskich lasach

Mieczysław Kołodziejczyk

**Automated measuring devices for pendulum wire displacements** ..... 39

Urządzenia do automatycznego pomiaru przemieszczeń drutu wahadła

### **Reviewers of the journal „Geoinformation Issues”**

The Editor would like to thank all the scientists who supported the journal by serving as referees for the manuscripts submitted to the journal „Geoinformation Issues” Vol. 7.

Marcin Barlik, Warsaw University of Technology, Poland

Andrzej Ciołkosz, professor emeritus, Poland

Kazimierz Ćmielewski, Wrocław University of Environmental and Life Sciences, Poland

Mieczysław Kwaśniak, Warsaw University of Technology, Poland

Xing Lelin, Wuhan University, China

Andrzej Mazur, Institute of Meteorology and Water Management, Poland

Grzegorz Mirek, Cracow University of Technology, Poland

Katarzyna Osińska-Skotak, Warsaw University of Technology, Poland

Wolfgang Söhne, Bundesamt für Kartographie und Geodäsie, Germany

# On the selection of GRACE-based GGMs and a filtering method for estimating mass variations in the Earth system over Poland

---

Walyeldeem Godah

Institute of Geodesy and Cartography, 27 Modzelewskiego St., 02-679, Warsaw, Poland  
Tel.: +48 22 3291903, Fax: +48 22 3291950, E-mail: walyeldeem.godah @igik.ed.pl

Malgorzata Szelachowska

Institute of Geodesy and Cartography, 27 Modzelewskiego St., 02-679, Warsaw, Poland  
Tel.: +48 22 3291903, Fax: +48 22 3291950, E-mail: malgorzata.szelachowska@igik.ed.pl

Jan Krynski

Institute of Geodesy and Cartography, 27 Modzelewskiego St., 02-679, Warsaw, Poland  
Tel.: +48 22 3291904, Fax: +48 22 3291950, E-mail: jan.krynski@igik.ed.pl

**Abstract:** Since the launch of the GRACE (Gravity Recovery And Climate Experiment) satellite mission in 2002, significant progress in the knowledge regarding the temporal variations of the Earth's gravity field has been achieved. The main objectives of this contribution are to define a suitable filter to reduce the noise contained in the latest release, i.e. RL05, of GRACE-based GGMs as well as to select the most suitable GRACE-based GGM time series for estimating mass variations in the Earth system over Poland. The performance of the Gaussian filter with different radii and the de-correlation filters (DDK1–DDK5) applied to reduce the noise contained in those GGMs was examined. First, they were investigated globally. Then, they were examined over the area of Poland, in particular, over two basins, i.e. the Vistula river basin and the Odra river basin. Moreover, both the internal and external accuracy of RL05 GRACE-based GGMs were assessed. Error degree variances of geoid heights were calculated on the basis of these models. Equivalent water thickness variations obtained from GRACE-based GGMs were compared with the corresponding ones obtained from the hydrology model. The obtained results were analysed and discussed. Finally the filtering method and the GGM time series most suitable for estimating mass variations in the Earth system over Poland were selected.

**Keywords:** GRACE, GGM, filter, equivalent water thickness

---

*Received: 9 February 2016 /Accepted: 17 March 2016*

## 1. Introduction

The Gravity Recovery and Climate Experiment (GRACE) satellite mission was launched in March 2002 by the US National Aeronautics and Space Administration (NASA) and the German Aerospace Centre (DLR). The primary goal of GRACE is to accurately map temporal variations of the Earth's gravity field at ~30 day intervals (e.g. Tapley et al., 2004). The mission is expected to be in operation until 2018 (e.g. Tapley et al., 2015). Research on the usefulness of GRACE data to study temporal mass variations in the Earth system has already been conducted by numerous teams worldwide

(e.g. Tapley et al., 2004; Chambers, 2006; Swenson and Wahr, 2007; Luthcke et al., 2013; Krynski et al., 2014; Wu and Helfin, 2015). For the area of Poland and surrounding areas the temporal variations of the Earth's gravity field, in terms of geoid height as well as mass variations, using Release 4 (RL04) GRACE-based Global Geopotential Models (GGMs) were investigated by Krynski et al. (2014). The authors showed that the amplitudes of geoid height variations for the area of Central Europe reach up to 7 mm. They also investigated the suitability of RL04 GRACE-based GGMs datasets and the filtering method applied to these GGMs. They concluded that the DDK1 filter and GGMs developed

by the JPL (Jet Propulsion Laboratory) centre were suitable for estimating mass variations in the Earth system over Central Europe. Birylo and Nastula (2012a) focused on filters applied to reduce the noise contained in RL04 GRACE-based GGMs. Their work indicated the superiority of the Anisotropic Non-symmetric filter (cf. Klees et al., 2008) for reducing the noise contained in those GGMs. Further, Birylo and Nastula (2012b) investigated the use of RL04 GRACE-based GGMs for predicting river flooding in Poland. Recently, Birylo et al. (2015) continued the investigation on GRACE-based GGMs. They studied the combination of these GGMs as well as combined GRACE and GOCE (Gravity field and steady-state Ocean Circulation Explorer; ESA, 1999) GGMs with metrological models for modelling flood risks over Poland.

During the GRACE mission, several groups of solutions for GRACE-based GGMs were developed: Release 1, Release 2, Release 3, Release 4, and the latest Release 5 (RL05). The solutions provided by computational centres were consequently improving, leading to better and better results (Dahle et al., 2014). The GGMs developed on the basis of GRACE data are strongly affected by noise due to the mission characteristics, in particular, the orbit configu-

ration (Tapley et al., 2004). This noise appears as meridional stripes in the final gravity field functionals determined from GRACE-based GGMs. Application of a suitable filter may substantially minimize that noise (the meridional stripes) contained in GRACE data (Ditmar et al., 2012). On the other hand, the applied filter should leave as much as possible of the gravity signal that allows reliable analysis of temporal variations of the gravity field functional to be conducted. The Gaussian filter has frequently been used as a standard due to its easy implementation and intuitive interpretation (Wahr et al., 1998). However, more recent works tend to apply probabilistic de-correlation methods in the post-processing of GRACE solutions, usually in conjunction with additional smoothing. The idea behind the de-correlation is to identify and remove error correlation in the sets of spherical harmonic coefficients using an a priori synthetic model of the observation geometry (Kusche et al., 2009). The main objectives of this contribution are to define a suitable filter to reduce the noise contained in the latest release, i.e. RL05, GRACE-based GGMs as well as to select the most suitable GRACE-based GGM time series for estimating mass variations in the Earth system over Poland.

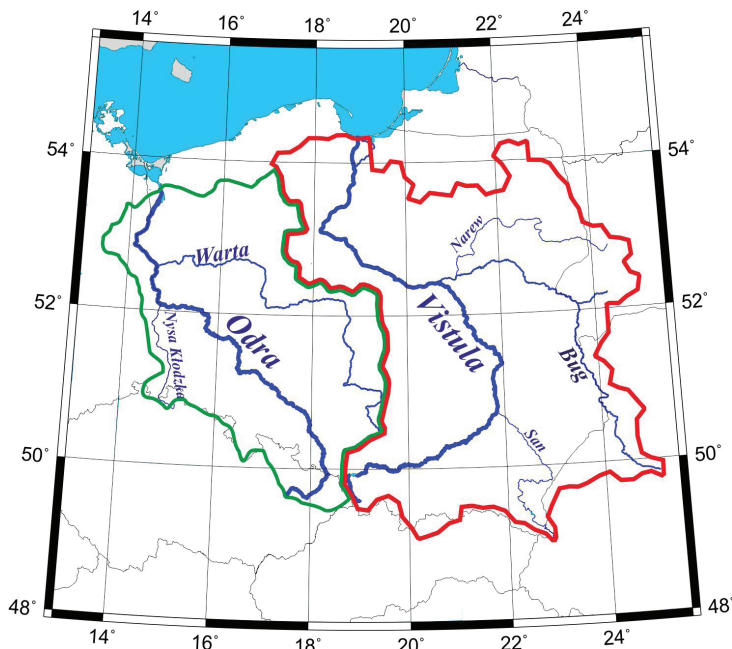


Fig. 1. The Vistula river basin (red polygon) and the Odra river basin (green polygon) in the study area

## 2. Study area and data used

### 2.1 Study area

The area of Poland was chosen as the main study area. In this area two main river basins are distinguished: the Vistula river basin, and the Odra river basin (Fig. 1). The Vistula river basin covers an area of ~194 424 km<sup>2</sup> while the area covered by the Odra river basin is about 118 861 km<sup>2</sup>.

### 2.2 Data used

The GGMs computed on the basis of GRACE data from 30 day time intervals are made available by several computational centres, i.e. the GFZ (Geo-ForschungsZentrum), the CSR (Centre for Space Research) and the JPL as well as by some other

scientific teams, e.g. the ITG (Institut für Geodäsie und Geoinformation of Bonn University), the DMT-1 (Delft University of Technology – Release 1), the AIUB (Astronomical Institute of Bern University), the CNES/GRGS (Centre National d'Etudes Spatiales/The Space Geodesy Research Group), the ULux (University of Luxembourg) and the Tongji (Tongji University). Several releases of GRACE-based GGMs were elaborated. The CSR, GFZ, and JPL were identified in the mission proposal as the GRACE Science Data System. They were considered as the official continuously releases monthly GRACE-based GGMs (cf. Bettadpur, 2012; Dahle et al., 2014; Watkins and Yuan, 2014). Moreover, the CSR, GFZ and JPL GRACE-based monthly GGMs cover a longer period compared to other scientific teams. Thus, in this study, the focus will be on the latest, i.e. RL05, GRACE-based GGMs

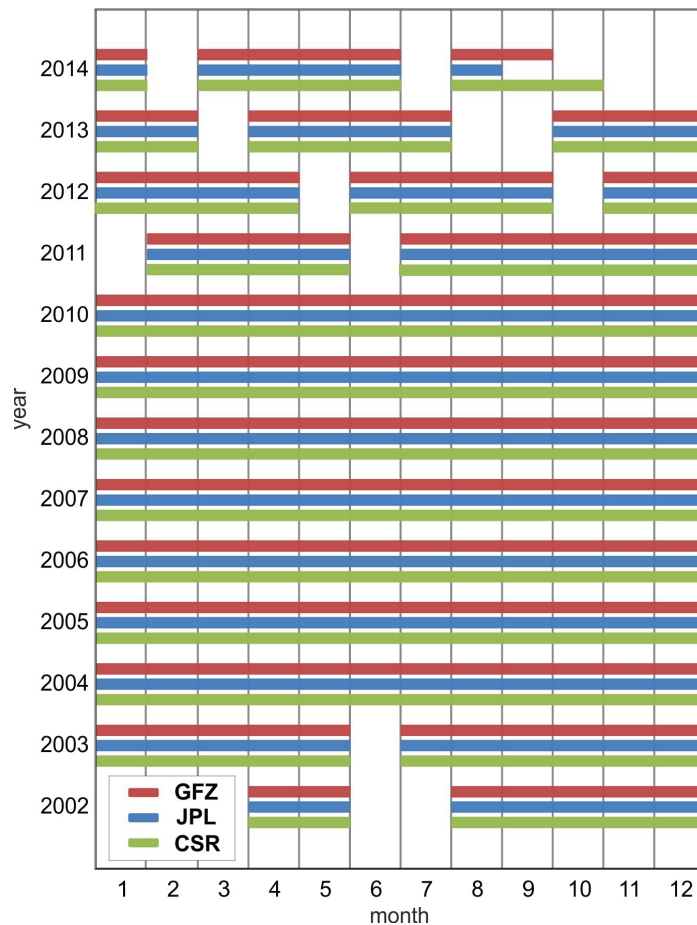


Fig. 2. Availability of RL05 GRACE-based GGMs from the CSR, GFZ, and JPL centres

from the CSR, GFZ, and JPL centres. They are released on the ICGEM (International Centre for Global Earth Models) website <http://icgem.gfz-potsdam.de/ICGEM/ICGEM.html>. The availability of these GGMs is shown in Figure 2. Most of the gaps in the GGM time series are common for the computational centres considered. The spatial resolutions of RL05 GRACE-based GGMs developed by the GFZ and the CSR centres are up to d/o 90 and d/o 96, respectively. The spatial resolutions of RL05 GRACE-based GGMs developed by the JPL centre are not uniform. They vary from d/o 60 to d/o 90.

The WaterGAP (Water Global Assessment and Prognosis) Global Hydrological Model (WGHM) developed by the research team from the University of Kassel and the University of Frankfurt, Germany was used for the evaluation of GRACE-based GGMs. This model is based on global hydrological and metrological datasets as well as a  $0.5^\circ \times 0.5^\circ$  spatial resolution of monthly runoff and river discharge (see Döll et al., 2003). The WGHM used in this study was obtained, in the form of monthly  $1^\circ \times 1^\circ$  grids, from the DFG (Deutsche Forschungsgemeinschaft) priority programme – *Mass Transport and Mass Distribution in the Earth System*.

### 3. Methodology

In the first part of this study, the effect of using different filtering methods on RL05 GRACE-based GGMs was examined. Gaussian filters with different radii as well as the de-correlation filters (i.e. DDK filters) were applied (cf. Wahr et al., 1998; Kusche, 2007; Kusche et al., 2009). The equivalent water thickness ( $EWT$ ) values were computed at monthly intervals using RL05 GRACE-based GGMs as follows (Wahr et al., 1998):

$$EWT^{(GRACE)} = \frac{R \times \rho_{av}}{3} \sum_{n=0}^{N_{max}} \left( \frac{2n+1}{1+k_n} \right) \sum_{m=0}^n \bar{Y}_m(\varphi, \lambda) \quad (1)$$

with

$$\bar{Y}_{nm}(\varphi, \lambda) = (C_{nm} \cos m\lambda + S_{nm} \sin m\lambda) \bar{P}_{nm}(\sin\varphi) \quad (2)$$

where  $\varphi, \lambda$  are the latitude and the longitude, respectively, of the computation point  $P$ ,  $N_{max}$  is the applied maximum degree of the GRACE-based GGM,  $R$  is the Earth's mean radius,  $\rho_{av}$  is the average density of the Earth,  $k_n$  are load Love numbers,  $C_{nm}, S_{nm}$  are

dimensionless coefficients of degree  $n$  and order  $m$ ,  $\bar{P}_{nm}(\sin\varphi)$  are fully normalized associated Legendre functions.

The temporal variations of the equivalent water thickness  $\Delta EWT^{(GRACE)}$  from RL05 GRACE-based GGMs were computed as follows:

$$\Delta EWT_i^{(GRACE)} = EWT_i^{(GRACE)} - EWT_{mean}^{(GRACE)} \quad (3)$$

where  $EWT_i^{(GRACE)}$  represents the equivalent water thickness obtained from RL05 GRACE-based GGMs,  $i$  denotes the month,  $EWT_{mean}^{(GRACE)}$  is the mean value obtained from the time series of  $EWT_i^{(GRACE)}$ .

In order to select the most suitable RL05 GRACE-based GGM time series for estimating mass variations in the Earth system over Poland, both the internal accuracy and the external accuracy of RL05 GRACE-based GGMs were investigated. The internal accuracy of these GGMs was evaluated using the error degree variances for geoid heights  $\varepsilon_N$  calculated as follows (Pavlis, 1988):

$$\varepsilon_N^2 = \left( \frac{GM}{\gamma a} \right)^2 \left( \frac{a^2}{R^2} \right)^{n+1} \sum_{m=0}^n \left( \varepsilon_{C_{nm}}^2 + \varepsilon_{S_{nm}}^2 \right) \quad (4)$$

where  $\varepsilon_{C_{nm}}, \varepsilon_{S_{nm}}$  are errors of spherical harmonic coefficients of RL05 GRACE-based GGMs, and  $a$  is the semimajor axis of the reference ellipsoid.

The external accuracy of these GGMs was examined using independent datasets. For this purpose, the temporal variations of the equivalent water thickness were computed from the WGHM as follows:

$$\Delta EWT_i^{(WGHM)} = EWT_i^{(WGHM)} - EWT_{mean}^{(WGHM)} \quad (5)$$

where  $EWT_i^{(WGHM)}$  represents the equivalent water thickness obtained from the WGHM monthly grids,  $EWT_{mean}^{(WGHM)}$  is the mean value obtained from time series of  $EWT_i^{(WGHM)}$ . These  $\Delta EWT_i^{(WGHM)}$  were compared with the corresponding  $\Delta EWT_i^{(GRACE)}$  obtained from RL05 GRACE-based GGMs. The differences  $d\Delta EWT_i$  between those equivalent water thickness variations are obtained as follows:

$$d\Delta EWT_i = \Delta EWT_i^{(WGHM)} - \Delta EWT_i^{(GRACE)} \quad (6)$$

### 4. Results and analysis

First, the performance of Gaussian filters of different radii and de-correlation filters (DDK1–DDK5) in a global scale was investigated. The results were

basically obtained with the use of Eq. (1) and Matlab codes developed by the DFG. Figure 3 illustrates the equivalent water thickness variations between March 2005, and September 2005 obtained from RL05 GRACE-based GGMs computed by the JPL centre. It shows that among all filters investigated, the DDK1 filter and the Gaussian filter with a radius of 700 km substantially reduce the noise contained in RL05 GRACE-based GGMs. The amplitudes of equivalent water thickness variations ranged from  $-48$  cm to  $25$  cm and from  $-66$  cm to  $31$  cm after applying the Gaussian filter with a radius of 700 km and the DDK1 filter, respectively. This indicates that the Gaussian filter removed 24 cm more of equivalent water thickness variations signal than the DDK1 filter. Therefore, it can be concluded that the DDK1 filter is more suitable than other

filters applied to reduce the noise contained in RL05 GRACE-based GGMs.

Then, the performance of using Gaussian filters of different radii and de-correlation filters (DDK1–DDK5) was investigated in a local/regional scale, in particular, over the Vistula river basin and the Odra river basin. Most of the results were obtained using the ICGEM calculation services (cf. <http://icgem.gfz-potsdam.de/ICGEM/ICGEM.html>). Figure 4 illustrates time series of equivalent water thickness variations  $\Delta EWT^{(GRACE)}$  for those river basins. It shows that the differences between CSR, GFZ, and JPL RL05 GRACE-based GGMs are merely negligible when applying DDK1 and DDK2 filters. The results presented in Figure 4 also indicate clear pattern of seasonal water mass variations, with the maximum values in March and minimum

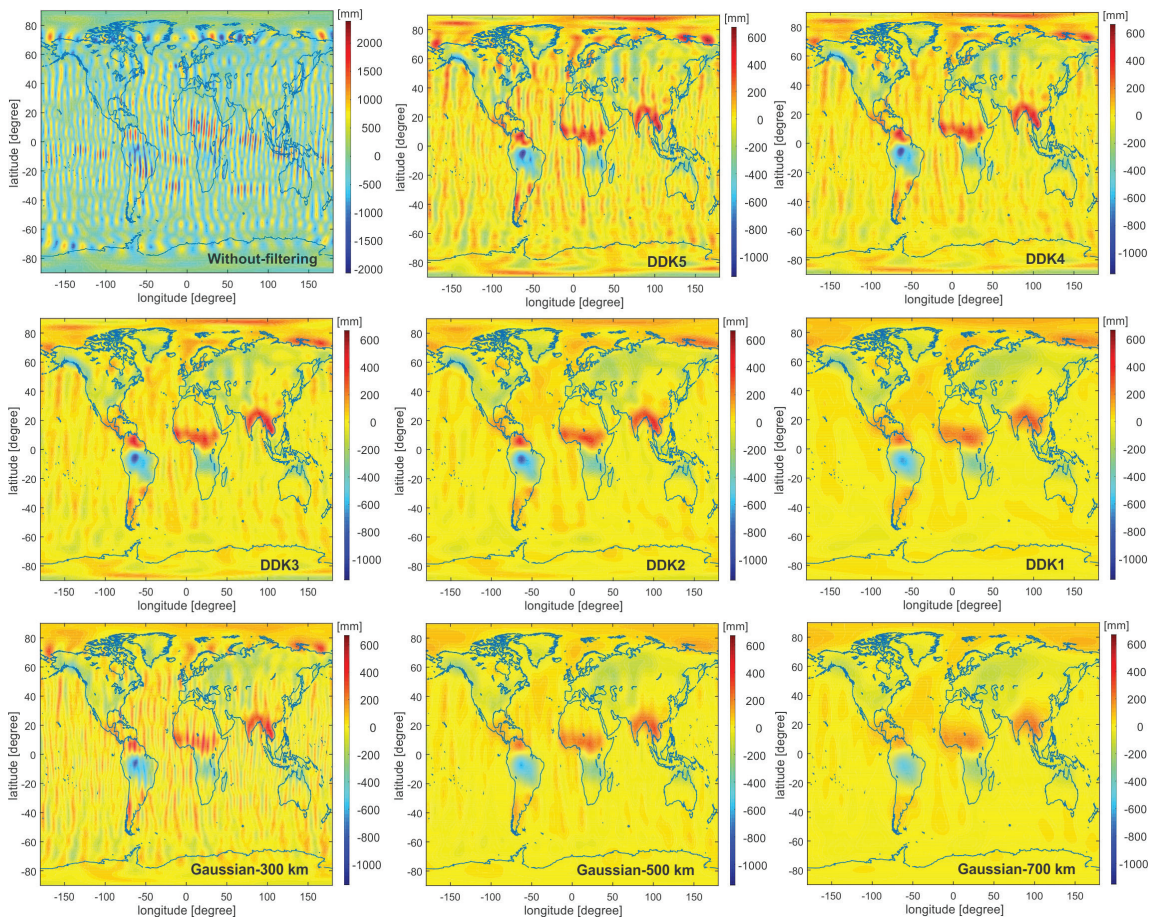


Fig. 3. The equivalent water thickness variations between March 2005 and September 2005 obtained from RL05 GRACE-based GGMs computed by the JPL centre

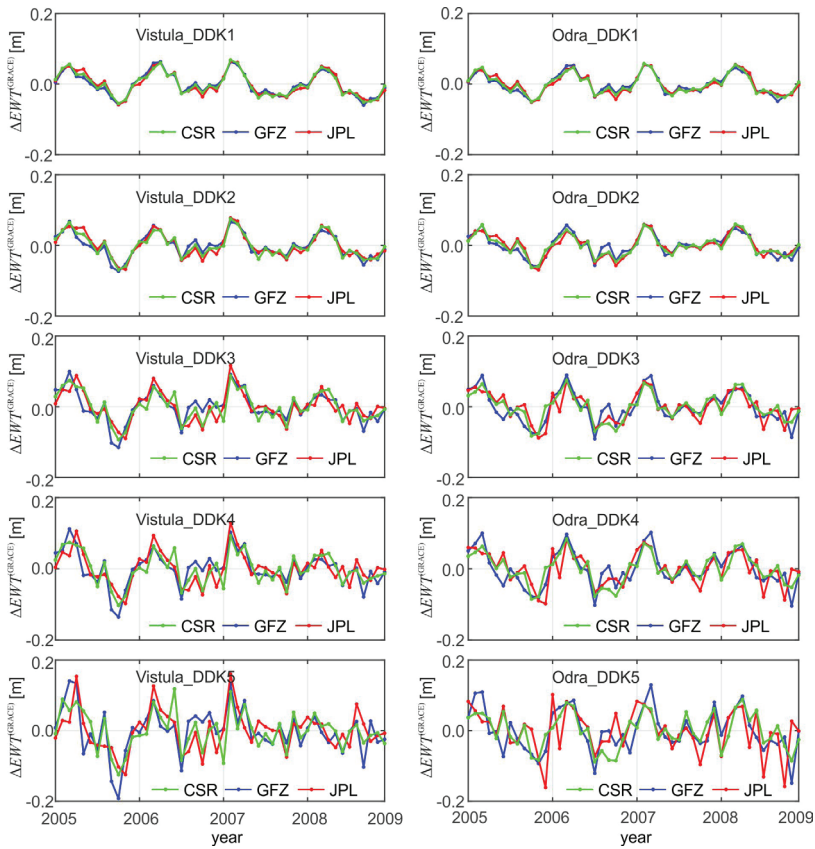


Fig. 4a. Time series of  $\Delta EWT^{(GRACE)}$  for the Vistula river basin (left panels) and the Odra river basin (right panels) using DDK1, DDK2, DDK3, DDK4, and DDK5 filters

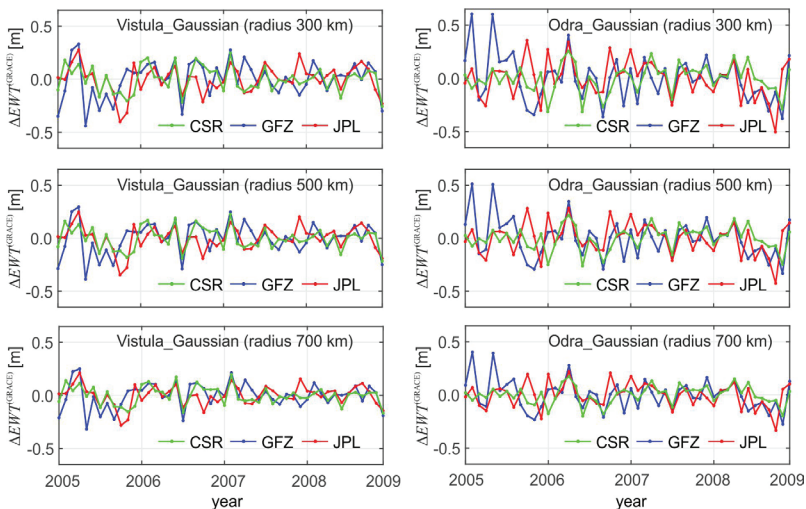


Fig. 4b. Time series of  $\Delta EWT^{(GRACE)}$  for the Vistula river basin (left panels) and the Odra river basin (right panels) using Gaussian filters with radii of 300 km, 500 km, and 700 km

values in July–September. This pattern of seasonal water mass variations may reveal that the increases/decreases in water masses over the area investigated are due to the melting of snow that was accumulated in the winter season, and water evaporation during dry months in the summer season. On the other hand, when applying DDK3, DDK4, DDK5 filters and Gaussian filters for all radii investigated, differences between  $\Delta EWT^{(GRACE)}$  obtained from CSR, GFZ, and JPL RL05 GRACE-based GGMs became visible. Furthermore, the pattern of seasonal water mass variations of  $\Delta EWT^{(GRACE)}$  cannot be clearly observed when applying the latter filters. This may indicate that the noise remaining, after applying the DDK3, DDK4, DDK5 filters and Gaussian filters for all radii investigated, dominates the  $\Delta EWT^{(GRACE)}$  signal. These results were obtained for the Vistula river basin and the Odra river basin, separately. They show that RL05 GRACE-based GGMs allow the estimation of mass variations in the Earth system for each of these basins independently. The results obtained may also reveal that the DDK1 and DDK2 filters are recommended to reduce the noise contained in RL05 GRACE-based GGMs, when estimating mass variations in the Earth system over Poland. This consequence agreed with the one presented in Krynski et al. (2014), which revealed that the DDK1 filter reduced the noise contained in release 4 GRACE-based GGMs sufficiently. Thus, the DDK1 filter was chosen as the best filter to perform further analysis in this contribution.

The errors of the spherical harmonic coefficients of RL05 GRACE-based GGMs developed by the

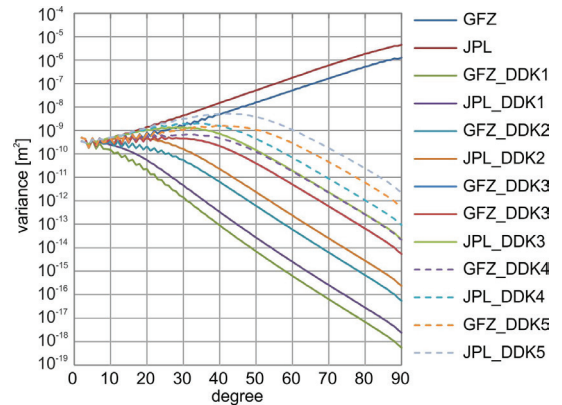


Fig. 5. The error degree variances for geoid heights from RL05 GRACE-based GGMs

CSR centre are not available, thus the internal accuracy of RL05 GRACE-based GGMs developed only by GFZ and JPL centres was examined. With the use of Eq. (4), the error degree variances for geoid heights were calculated for RL05 GRACE-based GGMs for the period from January 2008 to December 2009. Figure 5 shows the mean values of error degree variances for geoid heights for that period. The results presented in Figure 5 revealed that RL05 GRACE-based GGMs developed by the GFZ centre are more accurate than the ones developed by the JPL centre. This may be due to the essential improvement in developing GRACE-based GGMs from RL04 to RL05 by the GFZ centre (see Dahle et al., 2014).

The  $\Delta EWT^{(GRACE)}$  obtained from RL05 GRACE-based GGMs filtered with the use of the DDK1 filter were compared with the corresponding  $\Delta EWT^{(WGHM)}$

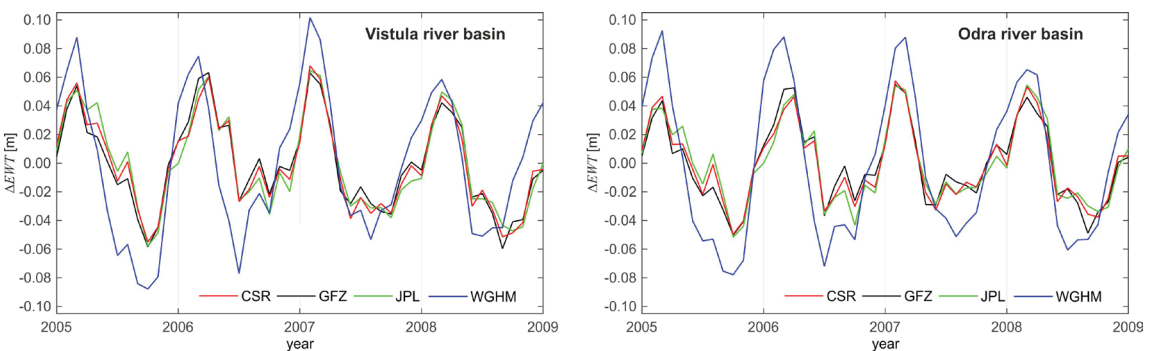


Fig. 6. Time series of equivalent water thickness variations  $\Delta EWT^{(WGHM)}$  and  $\Delta EWT^{(GRACE)}$  for the Vistula river basin and the Odra river basin

obtained from the WGHM monthly grid over the Vistula river basin and Odra river basin. Figure 6 illustrates time series of equivalent water thickness variations  $\Delta EWT^{(GRACE)}$  and  $\Delta EWT^{(WGHM)}$  for the Vistula river basin and the Odra river basin.

The results presented in Figure 6 show the pattern of seasonal water mass variations with maximum values of  $\Delta EWT$  in the spring months, while minimum values of those  $\Delta EWT$  are usually observed in July–September. This may justify the interoperation of the results concerning the increase/decrease in water masses over the investigated area (cf. Figure 4). Overall, the results presented in both Figures 4 and 6 may reveal that RL05 GRACE-based GGMs can be used sufficiently to estimate the temporal mass variations in the Earth system, e.g. equivalent water thickness variations, over Poland, in particular, over both the Vistula river basin and Odra river basin, independently.

The differences between  $\Delta EWT^{(WGHM)}$  and  $\Delta EWT^{(GRACE)}$  were computed using Eq. (6). Their statistics are given in Table 1. They indicate that RL05 GRACE-based GGMs provided by the GFZ centre are superior with respect to the other time series investigated, i.e. RL05 GRACE-based GGMs provided by the CSR and the JPL centres, in terms of standard deviation of the differences and the range of the differences. This result also agrees with the one presented in Figure 5. Thus, it can be concluded that for estimating mass variations in the Earth system over the area of Poland, RL05 GRACE-based GGMs developed by the GFZ centre are more recommended than the corresponding GGMs developed by CSR and JPL centres.

Table 1. Statistics of the differences between the corresponding equivalent water thickness variations  $\Delta EWT^{(WGHM)}$  and  $\Delta EWT^{(GRACE)}$  for the Vistula river basin and the Odra river basin [m]

Statistics	Vistula river basin			Odra river basin		
	GFZ	JPL	CSR	GFZ	JPL	CSR
Min	-0.067	-0.073	-0.070	-0.059	-0.063	-0.056
Max	0.047	0.048	0.046	0.053	0.065	0.059
Std	0.030	0.033	0.031	0.030	0.032	0.030
Max-Min	0.114	0.121	0.117	0.112	0.128	0.115

## 5. Conclusions

In this contribution, the applied filters to reduce the noise contained in the latest release of GRACE-based GGMs as well as the most suitable GRACE-based GGM time series for estimating mass variations in the Earth system over Poland were investigated.

In a global scale, both the DDK1 filter and the Gaussian filter with a radius of 700 km substantially reduce the noise in GRACE-based GGMs. Moreover, the results obtained show that the DDK1 filter recovers ~25% more of equivalent water thickness variations signal than the Gaussian filter with a radius of 700 km. This may indicate that the DDK1 filter is more suitable to reduce the noise contained in RL05 GRACE-based GGMs than other filters investigated.

In a local scale, in particular, over the area of Poland, the obtained results revealed that DDK1 and DDK2 filters seem more suitable than the Gaussian filter with a radius of 300 km, 500 km and 700 km as well as DDK3, DDK4, and DDK5 filters, to reduce the noise included in RL05 GRACE-based GGMs over the investigated area. This result agrees with that of a previous investigation concerning the selection of the best filtering method to reduce the noise contained in RL04 GRACE-based GGMs (cf. Krynski et al., 2014).

The comparison between error degree variances for geoid heights for RL05 GRACE-based GGMs from GFZ and JPL centres suggests that the GGMs developed by the GFZ centre are more accurate than the corresponding ones developed by the JPL centre. Moreover, over the area of Poland, the comparison between equivalent water thickness variations obtained from RL05 GRACE-based GGMs and the corresponding ones obtained from the WGHM revealed the superiority of RL05 GRACE-based GGMs developed by the GFZ centre to estimate temporal mass variations in the Earth system over Poland, over other GGM time series investigated.

## Acknowledgements

This work was supported by the Polish National Science Centre (NCN) within the research grant No 2014/13/B/ST/10/02742. The WGHM data and

some Matlab codes used in this study provided by the DFG SPP1257 “Mass transport and mass distribution in the Earth’s system” are acknowledged.

## References

- Bettadpur S., (2012): *UTCSR Level-2 Processing Standards Document for Level-2 Product Release 0005*, GRACE 327–742, CSR Publ. GR-12-xx, Rev. 4.0, University of Texas at Austin, pp. 16.
- Birylo M., Nastula J., (2012a): *Local Equivalent Water Thickness Determination as a Source of Data for Flood Phenomenon Observation*, Papers on Global Change IGBP 19(1), pp. 43–52, ISSN (Print) 1730-802X, doi: 10.2478/v10190-012-0003-8
- Birylo M., Nastula J., (2012b): *Signal Filtering as a Means of Determining Equivalent Water Thickness in Poland*, Papers on Global Change, 19(1), pp. 33–42.
- Birylo M., Nastula J., Kuczynska-Siehien J., (2015): *The creation of flood risk model using a combination of satellite and meteorological models*, Acta Geodyn. Geomaterialia, 12, 2(178), pp. 151–156.
- Chambers D.P., (2006): *Evaluation of new GRACE time-variable gravity data over the ocean*, Geophys. Res. Lett., 33(17), doi:10.1029/2006GL027296
- Dahle C., Flechtner F., Gruber C., König D., König R., Michalak G., Neumayer K.H., (2014): *GFZRL05: An Improved Time-Series of Monthly GRACE Gravity Field Solutions*, Observation of the System Earth from Space – CHAMP, GRACE, GOCE and future missions, Advanced Technologies in Earth Sciences, pp. 29–39, Doi: 10.1007/978-3-642-32135-1\_4
- Ditmar P., Teixeira da Encarnação J., Farahani H.H., (2012): *Understanding data noise in gravity field recovery on the basis of inter-satellite ranging measurements acquired by the satellite gravimetry mission GRACE*, J Geod. 87(9), pp. 1–25, doi:10.1007/s00190-011-0531-6
- Döll P., Kaspar F., Lehner B., (2003): *A global hydrological model for deriving water availability indicators: model tuning and validation*, Journal of Hydrology, 270 (1–2), pp. 105–134.
- ESA, (1999): *Gravity Field and Steady-State Ocean Circulation Mission*, Report for mission selection of the four candidate Earth Explorer missions, ESA SP 1233(1).
- Jolliffe I.T., (2002): *Principal Component Analysis*, 2<sup>nd</sup> edition, Springer, New York.
- Klees R., Rervtova E.A., Gunter B., Ditmar P., Oudman E., Winsemius H.C., Savanije H.H., (2008): *The design of an optimal filter for monthly grace gravity field models*, Geophys. J. Int. 175: pp. 417–432, doi: 10.1111/j.1365-246X.2008.03922.x
- Krynski J., Kloch-Glowka G., Szelachowska M., (2014): *Analysis of time variations of the gravity field over Europe obtained from GRACE data in terms of geoid height and mass variations*, In: C. Rizos and P. Willis (Eds.), Earth on the Edge: Science for a Sustainable Planet, International Association of Geodesy Symposia 139: pp. 365–370.
- Kusche J., Schmidt R., Petrovic S., Rietbroek R., (2009): *Decorrelated GRACE time-variable gravity solutions by GFZ, and their validation using a hydrological model*, J. Geod. 83(10): pp. 903–913.
- Kusche J., (2007): *Approximate decorrelation and non-isotropic smoothing of time variable GRACE-type gravity field models*, J. Geod. 81(11), pp. 733–749.
- Luthcke S.B., Sabaka T.J., Loomis B.D., Arendt A.A., McCarthy J.J., Camp J., (2013): *Antarctica, Greenland and Gulf of Alaska land-ice evolution from an iterated GRACE global mascon solution*, J. Glaciol., 59(216), pp. 613–631, doi: 10.3189/2013JoG12J147
- Pavlis N.K., (1988): *Modeling and estimation of a low degree geopotential model from terrestrial gravity data*, Rep. 386, Dept. of Geod. Sci. and Surv., Ohio State Univ., Columbus.
- Rangelova E., van der Wal W., Braun A., Sideris M.G., Wu P., (2007): *Analysis of Gravity Recovery and Climate Experiment time-variable mass redistribution signals over North America by means of principal component analysis*, J. Geophys. Res. 112, F03002. doi:10.1029/2006JF000615
- Swenson S., Wahr J., (2007): *Multi-sensor analysis of water storage variations in the Caspian Sea*, Geophys. Res. Lett., 34, L16401, doi:10.1029/2007GL030733
- Tapley B., Flechtner F., Watkins M., Bettadpur S., (2015): *GRACE Mission: Status and Prospects*, The GRACE Science Team Meeting, 21–23 Sept. 2015, Austin, Texas.
- Tapley B.D., Bettadpur S., Watkins M., Reigber C., (2004): *The gravity recovery and climate ex-*

- periment: Mission overview and early results*, Geophys. Res. Lett. 31, L09607, doi: 10.1029/2004GL019920
- Wahr J., Molenaar M., Bryan F., (1998): *Time variability of the Earth's gravity field: Hydrological and oceanic effects and their possible detection using GRACE*, J. Geophys. Res., 103(B12), pp. 30205–30229.
- Watkins M.M., Yuan D-N., (2014): *GRACE: JPL Level-2 Processing Standards Document for Level-2 Product Release 05.1*, GRACE 327–744 (v5.1), Jet Propulsion Laboratory, California Institute of Technology, pp. 14.
- Wu X., Heflin M.B., (2015): *A global assessment of accelerations in surface mass transport*, Geophys. Res. Lett., 42(16), pp. 6716–6723, doi: 10.1002/2015GL064941

## Wybór globalnych modeli geopotencjału opracowanych na podstawie danych z misji GRACE oraz metody filtracji, do wyznaczania zmian rozkładu mas w systemie Ziemia na obszarze Polski

Walyeldeen Godah

Instytut Geodezji i Kartografii, ul. Modzelewskiego 27, PL 02-679 Warszawa  
Tel.: +48 22 3291903, Fax: +48 22 3291950, E-mail: walyeldeen.godah @igik.ed.pl

Małgorzata Szelachowska

Instytut Geodezji i Kartografii, ul. Modzelewskiego 27, PL 02-679 Warszawa  
Tel.: +48 22 3291903, Fax: +48 22 3291950, E-mail: malgorzata.szelachowska@igik.ed.pl

Jan Kryński

Instytut Geodezji i Kartografii, ul. Modzelewskiego 27, PL 02-679 Warszawa  
Tel.: +48 22 3291904, Fax: +48 22 3291950, E-mail: jan.krynski@igik.ed.pl

**Streszczenie:** Satelitarna misja GRACE (Gravity Recovery And Climate Experiment zapoczątkowana w 2002 roku znacząco przyczyniła się do rozwoju wiedzy o zmianach w czasie pola siły ciężkości Ziemi. Głównym celem niniejszego opracowania jest zdefiniowanie odpowiedniego filtra do redukcji szumu zawartego w ostatniej wersji, tj. wersji 5. globalnych modeli geopotencjału opracowanych na podstawie danych z misji GRACE, jak również wybór najbardziej odpowiedniego szeregu czasowego globalnych modeli geopotencjału wyznaczonych na podstawie danych z misji GRACE, do określenia zmian rozkładu mas w systemie Ziemia dla obszaru Polski. W szczególności badano wpływ filtrów Gaussa o różnych promieniach oraz filtrów dekorelacyjnych (DDK1–DDK5) na redukcję szumu zawartego w globalnych modelach geopotencjału. Na początku wpływ użycia filtra był badany w ujęciu globalnym. Następnie wpływ ten został zbadany dla obszaru Polski – oddzielnie dla dorzeczy Wisły i Odry. Ponadto, została oszacowana zarówno wewnętrzna, jak i zewnętrzna dokładność wersji 5. globalnych modeli geopotencjału opracowanych na podstawie danych z misji GRACE. Obliczono wariancje błędów wysokości geoidy dla poszczególnych stopni badanych modeli. Zmiany ekwiwalentnej warstwy wody wyznaczone z globalnych modeli geopotencjału opracowanych na podstawie danych z misji GRACE zostały porównane z odpowiednimi zmianami otrzymanymi z modelu hydrologicznego. Wyniki poddano analizie i dyskusji. Ostatecznie wybrano metodę filtracji oraz szereg czasowy globalnych modeli geopotencjału najbardziej odpowiednie do oszacowania zmian rozkładu mas w systemie Ziemia dla obszaru Polski.

**Słowa kluczowe:** GRACE, globalny model geopotencjału, ekwiwalentna warstwa wody

# Comparison of techniques for Integrated Precipitable Water measurement in the polar region

---

Michał Kruczyk

Department of Geodesy and Geodetic Astronomy, Warsaw University of Technology  
Pl. Politechniki 1, 00-661, Warsaw, Poland  
Tel/Fax: +48 22 2347754, E-mail: [kruczyk@gik.pw.edu.pl](mailto:kruczyk@gik.pw.edu.pl)

**Abstract:** Tropospheric delay estimates (tropospheric product) for selected International GNSS Service (IGS) and EUREF Permanent Network (EPN) stations made it possible to assess two aerological techniques in the polar region (mainly in Greenland). Integrated Precipitable Water (IPW) – important meteorological parameter is derived from GPS tropospheric solutions by a known procedure for GPS stations. To convert from the wet part of tropospheric delay (ZWD) to IPW, the relation between 2 m temperature and the so-called mean temperature of the atmosphere above was derived using local radiosonde data for nearby GPS stations. Sunphotometer data were provided by AERONET (NASA AERosol ROBotic NETWORK). IPW comparisons lead to the determination of a systematic difference between the techniques of GPS IPW and sunphotometer data (not present in the case of RAOBs). IPW measured by sunphotometer CIMEL (Cimel Electronique) is several percent smaller than IPW from GPS (both IGS and EPN solution). The bias changes seasonally and is a function of atmospheric temperature. It signals some systematic deficiencies in solar photometry as the IPW retrieval technique. CIMEL IPW shows some temperature dependent bias also in relation to radiosoundings.

**Keywords:** water vapour, GNSS meteorology, precipitable water vapour, sunphotometer, radiosounding, polar research, Greenland

---

*Received: 24 January 2016 /Accepted: 13 March 2016*

## 1. Introduction

Water vapour is an extremely important component of the water cycle and plays a crucial role in many meteorological, climatological and environmental processes (such as evapotranspiration, condensation, precipitation, thermodynamic latent heat release, cloudiness and its impact on insolation, etc.) as acknowledged in numerous sources even at the textbook level (e.g. Shelton, 2009; McIlven, 2010; Salby, 2012). The average value of IPW for the Earth is about 25 mm but average precipitation amounts to about 1000 mm which exhibits clear evidence of high dynamics of hydrological processes (45 evaporation-condensation cycles in one year). Water vapour contributes to the greenhouse gas effect more than carbon dioxide (but of course lasts in the atmosphere for a short time). In a warmer atmosphere saturation water vapour

pressure is higher and likewise water vapour density for the same relative humidity. Water vapour is both climate change agent and indicator (see e.g. Kruczyk, 2014). Integrated precipitable water, i.e. column water content in the whole of the atmosphere, provides a convenient measure of water vapour and is obtained by means of measurements by a variety of techniques.

There are several completely different techniques to observe/measure water vapour content in the atmosphere:

- in-situ meteorological measurements (various thermohygrometers, capacity sensors etc.),
- radiosonde/dropsonde (direct measurements from the device moving through the atmosphere),
- Water Vapour Radiometry (WVR) – remote sensing possible both from ground and satellite platforms,
- LIDAR (especially Raman and DIAL types),

- Fourier Transform Infrared Spectrometry (FTIR),
- sun photometry (with a rare lunar variety),
- differential optical absorption spectrometry (DOAS),
- GNSS meteorology (described in detail below).

The main aim of this paper is to compare three of these techniques in the case of the polar region – Greenland. Here is a short description of the techniques tackled.

Atmospheric refraction of the Global Positioning System (GPS) L-band navigational signal manifests itself as tropospheric delay of pseudorange. For a GPS measurement taken for a satellite at zenith and a receiver located at sea level, the Zenith Tropospheric Delay (ZTD), in units of length, amounts to approximately 2.3 m. The ZTDs need to be properly taken into account when high accuracy of determined station coordinates is required, i.e. at the level of several millimetres. Due to limited accuracy of existing ZTD models, precise applications of GPS positioning (geodynamics, geodetic reference frames) require the estimation of ZTDs in the process of the adjustment of GPS observations, together with other parameters, like station coordinates, phase ambiguities, etc. (Hoffmann-Wellenhof et al., 2008; chapter 5.3). Because of temporal variability, ZTDs are usually estimated every hour for each station in the case of EPN (24 parameters for a daily session). For the IGS PPP solution there are 12 parameters each hour. Tropospheric delay is estimated together with coordinates. The GPS-derived ZTDs obtained from the networks of permanent GPS stations maintained for most precise scientific applications are also used for the purpose of atmospheric research and are the basis of GPS meteorology (Duan et al., 1996). ZTD is a sum of Zenith Wet Delay (ZWD) and Zenith Hydrostatic Delay (ZHD). ZWD, which is about 10% of ZTD, depends mostly on the content of water vapour along the path of signal propagation and is highly variable both spatially and temporally. ZHD depends mostly on surface atmospheric pressure, and can be computed at the several millimetre accuracy level from the existing ZHD models using surface meteorological data (Saastamoinen formula with gravitational correction as a function of surface atmospheric pressure is applied).

Integrated Precipitable Water (IPW) – sometimes denoted simply as PW – is a valuable meteorological parameter describing the quantity of water vapour in the vertical direction over the station in millimetres of liquid water after condensation. A related parameter – Integrated Water Vapour (IWV) – is also used; it has the same value as IPW but is expressed in another unit of measure, i.e. kg/m<sup>2</sup>. IPW can be calculated from ZTD by separating Zenith Hydrostatic Delay and Zenith Wet Delay before calculating IPW from previously obtained ZWD with the use of a numerical coefficient dependent on the so called “mean temperature” (along the vertical profile of the atmosphere) (Rocken et al., 1993; Bevis et al., 1994). The procedure is presented in detail in the next section.

On the other hand IPW can be determined from vertical humidity data, i.e. radiosounding data or numerical weather prediction models by integrating water vapour density. IPW can also be obtained from the measurements of atmospheric radiation in infrared using radiometers and photometers (see below). A number of studies have shown that IPW estimates from ground-based GPS observations and meteorological/aerological data give the same level of accuracy as aerological techniques. GNSS-derived IPW is the basis of a new discipline called GNSS meteorology, which is developing so dynamically and is such an abundant field for various types of research that it takes a full publication to present the state of the art (see e.g. Böhm and Schuh, 2013).

A number of studies have also shown that IPW estimates from ground-based GPS observations and meteorological/aerological data give the same level of accuracy as radiosondes and microwave radiometers (see e.g. Vedel et al., 2001). In this work both radiosoundings and another water vapour data source – sun photometer – are tested in exceptional conditions: at the polar region of Greenland.

The fundamental aerological technique is balloon soundings called radiosounding. GPS and RAOB comparisons in the form of ZTD are provided by Vedel in the frame of EPN (see the 2<sup>nd</sup> www in the References).

Integrated Precipitable Water for a radiosounding profile can be obtained by numerical integration of average water vapour density (calculated from temperature and relative humidity for each level  $j$

and averaged between registered levels, from surface reading  $j = 0$  up to the last level  $N$ ):

$$IPW = \sum_{k=1}^N \overline{\rho_{wv}(j-1, j)} (h_j - h_{j-1}) \quad (1)$$

CIMEL-318 sun photometer is an important tool in aerosol research (Halthorne et al., 1997; Holben et al., 1998; Holben et al., 2001). CIMEL is an automatic/robotic sun tracking photometer (solar powered) produced by Cimel Electronique ([www.cimel.fr](http://www.cimel.fr)). These multifunctional devices are operated in the framework of the AERONET (AERosol RObotic NETwork) programme coordinated by NASA and CNRS ([www.aeronet.net](http://www.aeronet.net)). The globally distributed network of over 100 sites provides assured aerosol optical properties to monitor atmosphere, environment and validate remote sensing satellite retrievals. A sun photometer is a multichannel radiometer which measures many air properties (mostly aerosols) registering absorption of 8 line bands of solar spectra (340, 380, 440, 500, 675, 870, 940 and 1020 nm nominal wavelengths; potentially also 1640 nm). The automatic Sun and sky scanning radiometers make direct Sun measurements with a  $1.2^\circ$  full FOV every 15 min. The direct Sun measurements take 8 seconds to scan all 8 wavelengths, with a motor driven filter wheel positioning each filter in front of the detector resulting in 3 measurements at each wavelength within a one minute period. These solar extinction measurements are then used to compute aerosol optical depth at each channel by means of comparing measurements of sky radiance with off-band wavelengths (with no absorption). CIMEL gives also IPW values (precisely – slant values in the direction to the Sun). The bandpass of ion assisted deposition interference filters (spectral windows breadth FWHM) of most channels is 10 nm and includes many individual lines of water vapour molecular spectral transitions (vibrational-rotational). Water vapour channels used by CIMEL are centred on 940 nm and 1020 nm (940 nm channel used solely to retrieve precipitable water). The relationship used to estimate the PW from the water vapour transmittance  $T_{wv}$  is:

$$T_{wv} = e^{-a(m \cdot IPW)^b} \quad (2)$$

The two constants  $a$  and  $b$  are related to the water vapour channel used and  $m$  is the relative optical airmass.

Spectrometric detection and measurements of water vapour (in this case called CWV – column water vapour) are demanding tasks because of the complexity of the instruments calibration (e.g. Schmid et al., 2001). CIMEL instruments use parameters (e.g. zero airmass voltages) from reference instruments calibrated at Mauna Loa Observatory every 3 months. From the point of view of GNSS meteorology CIMEL is an independent source of IPW.

Several investigations have been carried out to evaluate sunphotometer IPW by other techniques, also GNSS (see e.g. Pérez-Ramírez et al., 2014). They acknowledge the relatively low accuracy of IPW measured by sunphotometer (IPW bias of about 10%). There is ongoing work with the procedure of IPW retrieval from sunphotometer measurements (Alexandrov et al., 2009). Most comprehensive inter-technique comparison (dealing mostly with satellite devices) achieved better GNSS-CIMEL agreement but also reports some CIMEL IPW bias dependent on IPW value (Van Malderen et al., 2014).

There are several papers concerning GNSS meteorology in polar regions (see e.g. Vazquez and Brzezinska, 2012). The author performed investigations on IPW technique comparison in the case of a dedicated solution for a non-EPN station operated permanently (but not included in EPN) by the Institute of Geophysics of the Polish Academy of Sciences at Hornsund, Svalbard (Kruczyk and Liwosz, 2015).

## 2. GNSS tropospheric solutions and IPW determination

Several tropospheric solutions are routinely provided as a result of the International GNSS Service (IGS) and EUREF Permanent Network (EPN) services. In this research the author used the new IGS tropospheric product calculated by Byun and Bar-Sever, JPL, and from 2011 by Byram, USNO (see Byun and Bar-Sever, 2009) as well as the EPN (<http://www.epncb.oma.be>) standard product of the EPN network created as iterative weighted mean of individual analysis centres' solutions. The EPN combination (EUR) was made by Söhne (see Söhne and Weber, 2009) and Pacione (for details see: Pacione et al., 2011). The map in Figure 1 shows the location of analysed stations.

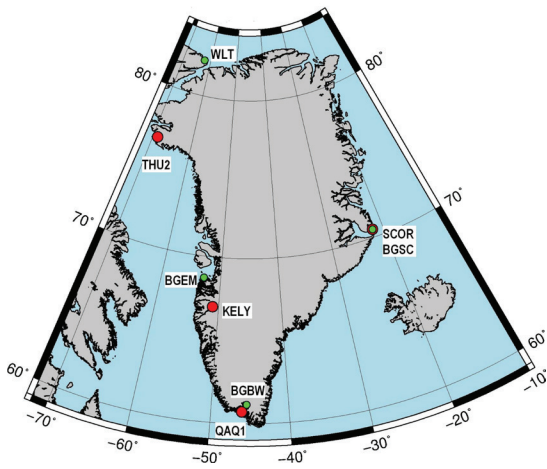


Fig. 1. GNSS stations used (red): THU2/THU3 – Thule, SCOR – Scoresbysund/ Ittoqqortoormiit, KELY– Kangerlussuaq and QAQ1 – Qaqortoq / Julianehaab and corresponding radiosounding points (green)

Integrated precipitable water, i.e. the total column of water vapour (as liquid) is determined from ZTD solution by a widely known procedure involving first the separation of Wet Delay by calculation of Hydrostatic Delay

$$ZWD = ZTD - ZHD \quad (3)$$

Physically ZHD is defined as follows:

$$ZHD = \int_0^{p_s} \frac{R_d k_1}{g} p \, dp \quad (4)$$

where  $p_s$  is the surface atmospheric pressure,  $R_d$  is specific gas constant for dry air,  $g$  is the acceleration of gravity, and empirical constant  $k_1 = 7.76 \cdot 10^{-7}$  [K/Pa]. In this work the Saastamoinen formula (Saastamoinen, 1972) with gravitational correction is used – ZHD is a function of surface atmospheric pressure

$$ZHD = 2.2779 \, p/f(\varphi, H) \quad (5)$$

where  $p$  is atmospheric pressure, function  $f$  reproduces changes in gravity with latitude  $\varphi$  and ellipsoidal height  $H$  in kilometres, and can be derived employing effective gravity and effective height (Davis et al., 1985)

$$f(\varphi, H) = (1 - 0.00266\cos 2\varphi - 0.00028H) \quad (6)$$

In the next step the obtained ZWD is transformed into IPW using the coefficient  $\kappa$  dependent on “mean temperature”

$$IPW \approx \kappa \cdot ZWD \quad (7)$$

with  $\kappa$  given as follows:

$$1/\kappa = 10^{-6}(k_3/T_m + k_2')R_v \quad (8)$$

where  $R_v$  is the specific gas constant for water vapour,  $T_m$  is “mean temperature” (through the vertical profile of atmosphere),  $k_i$  are empirical coefficients (given e.g. in: Davis et al., 1985). Coefficient  $\kappa$  of a value about 1/6.4 depends on temperature vertical profile but it can be estimated as a function of surface temperature at the GNSS station (Bevis et al., 1992).

$$T_m = \frac{\int_S (P_v/T) ds}{\int_S (P_v/T^2) ds} \approx \frac{\int_{h_0}^{\infty} (P_v/T) dh}{\int_{h_0}^{\infty} (P_v/T^2) dh} \quad (9)$$

One can model mean temperature as a linear function of surface temperature. Normally the linear model proposed by Bevis et al. (1992) is used; but in order to obtain higher accuracy it is better to use radiosounding profiles for the particular place. It is also possible to calculate  $T_m$  from a numerical weather prediction model. For example mean temperature is available at the Technical University of Vienna (for www see References) where they are computed from ECMWF (European Centre for Medium-Range Weather Forecasting) model operational analysis of pressure level data. As the IPW derivation procedure is quite sensitive to  $T_m$  values, the author used radiosounding data to obtain a local linear model for mean temperature (Table 1) as a function of surface atmospheric temperature  $T_s$  measured at the GNSS station at 2 m height. The polar tropopause, which is lower and relatively warmer in relation to the surface than tropopause for mid-latitudes makes the procedure particularly important in the case of polar stations. Soundings were performed in Greenland in the vicinity of 3 stations (at 207 km distance in the case of KELY); the nearest radiosounding point is in Northern Canada (Alert, Ellesmere Island, Nunavut). Figure 2 presents the fit of linear formula for two radiosounding stations in Greenland and the Bevis

Table 1. Mean temperature model for selected radiosounding points close to Greenland IGS/EPN stations, for the period of 2012–14

Radiosounding point	Nearby GNSS points	Distance [km]	Mean temperature formula [K] and difference STDEV	Number of radiosoundings
04339 BGSC Ittoqortoormiit	SCOR	1	$T_m = 62.2 + 0.74 \cdot T_s \pm 4.0$	2122
04270 BGBW Narsarsuaq	QAQ1	62	$T_m = 70.4 + 0.71 \cdot T_s \pm 4.4$	2158
04220 BGEM Aasiaat	KELY	206	$T_m = 12.1 + 0.92 \cdot T_s \pm 3.4$	2159
071082 WLT Alert (Nunavut, Canada)	THU2/THU3	675	$T_m = 96.0 + 0.62 \cdot T_s \pm 6.2$	2449

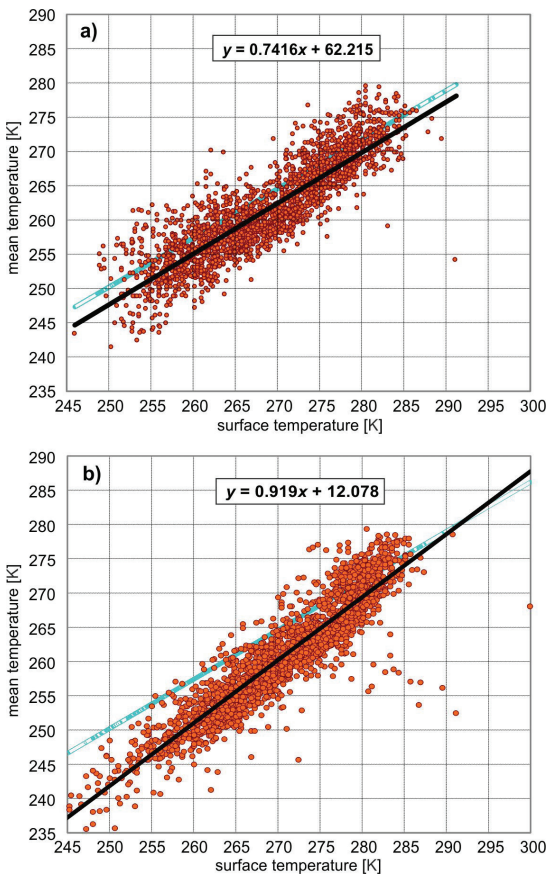


Fig. 2. Mean temperature vs. surface temperature for a) Ittoqortoormiit (04339 BGSC), and b) Aasiaat (04220 BGEM), 2012–2014 (2122 and 2159 soundings respectively), the fit of linear formula (black line) and Bevis formula (blue line)

formula (which has been obtained for lower latitudes of continental USA). The local formula is obviously better.

For the separation of ZWD direct measurements of meteorological parameters at GNSS stations are needed. Unfortunately the GNSS stations equipped with meteorological sensors are quite sparse (as for the Greenland stations local meteorological measurements are not provided for KELY).

Both meteorological data which are recorded in time intervals of 5 min, and ZTD estimates over 5 minute intervals (in the case of the IGS solution) have been averaged in hourly intervals to obtain IPW. Only hourly data are the subject of IPW comparisons described below.

Figure 3 shows annual series of IPW hourly values calculated from the IGS tropospheric solution

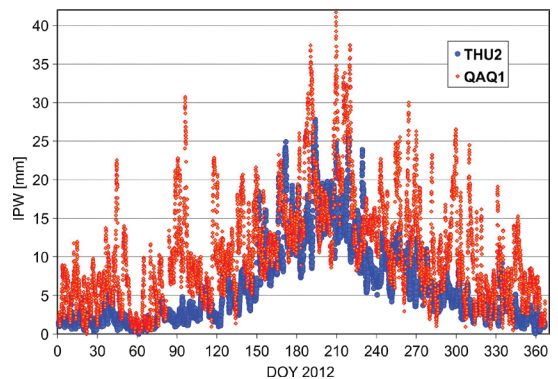


Fig. 3. Hourly GNSS IPW estimates in 2012 for THU2 (Thule) and QAQ1 (Ittoqortoormiit); IGS tropospheric product

for Thule (THU2) and Qaqortoq (QAQ1) – located at opposite sides of the giant island – in 2012. This graph even provides some details to describe the local climate: for QAQ1 (southern tip of Greenland) is much warmer and more variable than THU2 (far to the north). In polar regions IPW (if much smaller than in the tropics) exhibits strong seasonal and short time (i.e. several days) variability because of dramatic changes in insolation and influence of local atmospheric masses taking part in global circulation.

### 3. IPW from IGS/EPN tropospheric solutions and CIMEL sun-photometer comparisons

CIMEL automatic sun tracking photometers are operated in the framework of the AERONET programme in the vicinity of all four GNSS sites presented on the map in Figure 1. Unfortunately measurements at Narsarsuaq (near QAQ1) are seriously incomplete and measurements at Kangerlussuaq (near KELY) cannot be effectively used because meteorological measurements here are not available to precisely calculate IPW. To calculate IPW for GNSS site that does not record meteorological data one can use meteorological data from the sounding taking into account height difference or use some numerical weather prediction data. In such a case the precision needed to compare the techniques can never be achieved. For polar stations (especially Thule – far north of Greenland) CIMEL measurements are only possible when the Sun is high enough over the horizon – so only data (IPW measurements) for the period from the second half of March till late September are available (see Fig. 4).

IPW differences ( $\Delta$ IPW) for Thule will be investigated with the greatest attention because the techniques are almost collocated. The distance between CIMEL Thule and THU2/THU3 GNSS stations is only 2 km. Annually averaged results for both IGS and EPN solution in 6 subsequent years are listed in Table 2.

The sign of IPW difference (CIMEL – GPS) changes from positive to negative with growing IPW value (Fig. 5) also the histogram of differences is asymmetric (Fig. 6).

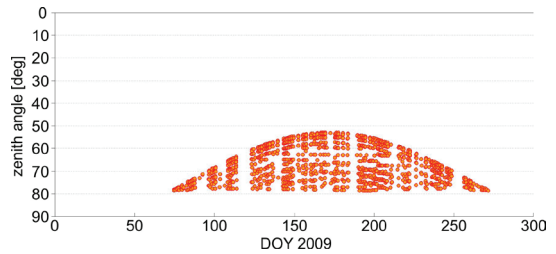


Fig. 4. Zenith angle of CIMEL measurements in 2009 at Thule ( $\varphi = 76.5^\circ$ )

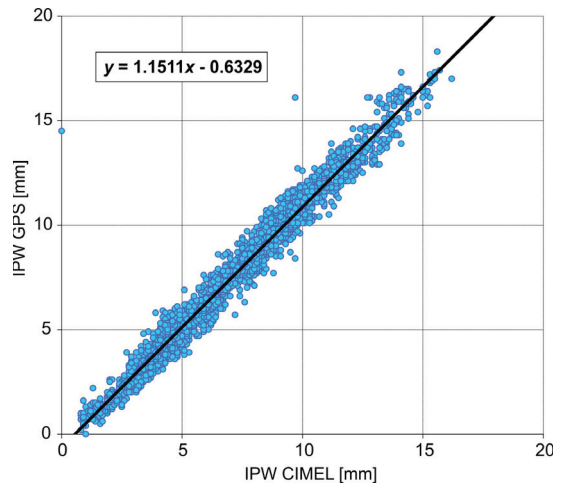


Fig. 5. IPW (CIMEL vs. GPS) for Thule (THU2) for 2009–2011

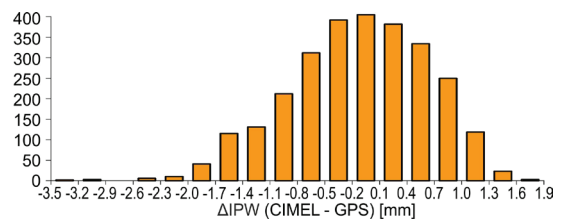


Fig. 6. IPW difference (CIMEL – GPS) for Thule (THU2) for 2009–2011 (2740 points)

The crucial point of this experiment – systematic annual change in IPW difference (between CIMEL-318 sunphotometer and IPW at GPS point) – is best illustrated in Figures 7 and 8. Annual averages (details in Table 2) and the scatterplot (Fig. 5) only suggest some inter-technique systematic bias, but time changes of IPW difference neatly follow seasons and temperature.

Table 2. Comparison of IPW from CIMEL and GPS at Thule (differences: CIMEL – GPS) EPN tropospheric combination and IGS tropospheric product (hourly averages of 5 minute estimates)

Year	GPS solution	IPW average difference [mm]	Difference STD [mm]	Difference RMS [mm]	GPS estimates	CSPHOT measurements
2009	THU2 IGS	-0.30	0.74	0.80	1247	3034
	THU3 IGS	-0.37	0.73	0.82	1177	2817
	THU3 EUR	-0.63	0.80	1.02	1202	2888
2010	THU2 IGS	-0.05	0.62	0.62	875	2184
	THU3 IGS	-0.12	0.62	0.63	888	2212
	THU3 EUR	-0.43	0.60	0.74	874	2176
2011	THU2 IGS	-1.23	0.62	1.38	618	1658
	THU3 IGS	-1.24	0.62	1.39	618	1658
	THU3 EUR	-1.30	0.66	1.46	618	1658
2012	THU2 IGS	-0.10	0.54	0.54	892	2865
	THU3 IGS	-0.12	0.55	0.56	892	2865
	THU3 EUR	-0.16	0.54	0.57	905	2915
2013	THU2 IGS	-0.60	0.80	1.00	1088	3294
	THU3 IGS	-0.54	0.73	0.91	1071	3285
	THU3 EUR	-0.63	0.72	0.96	1113	3403
2014	THU2 IGS	-0.88	0.76	1.16	858	2505
	THU3 IGS	-0.89	0.78	1.18	844	2470

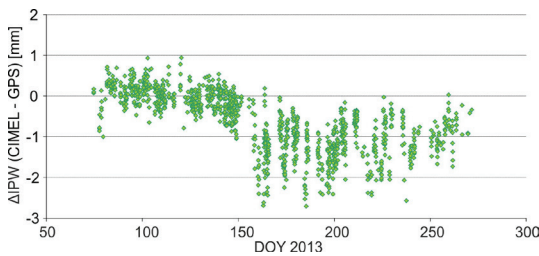


Fig. 7. IPW difference (CIMEL-GPS) for Thule (THU3) in 2013, EPN tropospheric combined solution; 1113 points

IPW difference has almost the same characteristics in two separate years, and two independent GPS solutions: EPN tropospheric product (combination of individual analysis centre standard network solutions (by Bernese 5.2) and IGS tropospheric product (PPP solution by GIPSY-OASIS). The only

difference is the number of simultaneous measurements available. Also THU2 shows almost identical results. Intriguing seasonal changes in IPW differences (CIMEL – GPS) can be best explained by the most obvious environmental factor – atmospheric temperature. There is clear dependence of IPW difference on temperature registered at GPS stations, best perceptible with a smaller number of points, i.e. during a single year (Fig. 9). There is no such dependence of IPW difference on zenith angle (its daily range also changes with season, Fig. 10).

Results presented clearly signal some systematic deficiencies in solar photometry as an IPW retrieval technique. Lack of IPW difference and zenith angle rather excludes a change in optical atmospheric properties as a possible cause. The probable reason for this phenomenon is a change in optical filter characteristics in sunphotometers working in extreme polar conditions. There is probably some

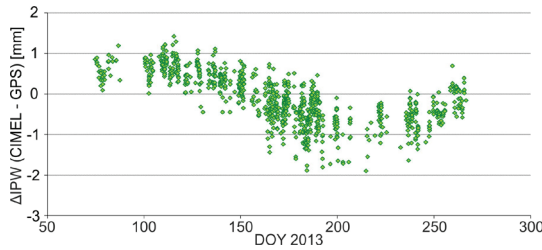


Fig. 8. IPW difference (CIMEL – GPS) for Thule (THU3) in 2010, IGS tropospheric solution

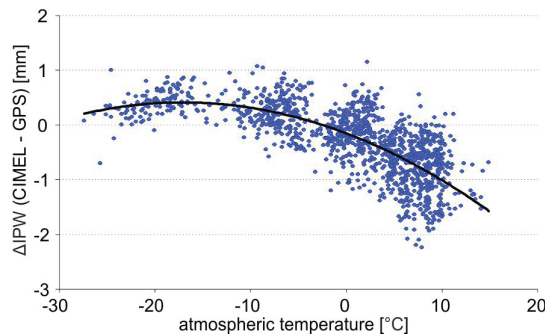


Fig. 9. IPW difference (CIMEL – GPS) for Thule (THU2) in 2009 as a function of atmospheric temperature, IGS tropospheric solution

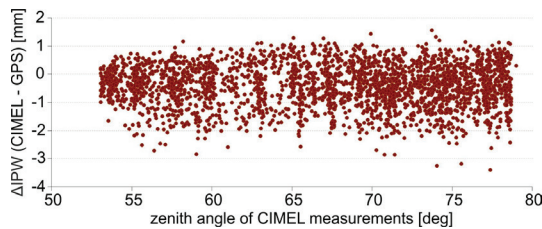


Fig. 10. IPW difference (CIMEL – GPS) for Thule (THU2) in 2009–2011 as a function of zenith angle of the Sun (CIMEL measurement), IGS tropospheric solution

change in the band pass filter characteristics in the non-thermostaticised device (A. Pietruczuk – personal communication).

Next the results are presented of an analogic comparison for CIMEL Ittoqqortoormiit and GPS at Scoresbysund (SCOR). This time the distance between CIMEL Ittoqqortoormiit and SCOR GNSS station is 9.7 km; the location is on the eastern side of Greenland at Greenland’s Sea shore.

Dependence of IPW differences on temperature both for Thule and Scoresbysund are put together in Figure 11. In both cases data from a 3 year period were used (for Thule the same period as in Figures 6 and 9). In the case of difference between Ittoqqortoormiit (CIMEL) and Scoresbysund (SCOR GNSS station) this effect (of temperature dependence of the IPW differences) is less conspicuous but still present. Points are located in Eastern Greenland (on the warmer side of the island) 6° of latitude to the south in relation to Thule – so less extreme temperatures are encountered there.

#### 4. GNSS IPW and sunphotometer IPW vs. radiosoundings

It is a common standard in GNSS meteorology to compare GPS IPW with radiosoundings. In this work the EPN combined tropospheric solution and IGS tropospheric product are the object of such a procedure.

There are two methods to compare IPW from the GNSS solution and radiosounding observations. First is to compare GNSS IPW obtained with local meteorological measurements (only where they are available). The second – possible for all GNSS stations near the radiosounding point – is to use surface meteorological readings from radiosounding to obtain IPW at the GNSS point taking into account the difference in orthometric heights. Hence one needs barometric correction to atmospheric pressure (see e.g. Andrews, 2010; chapter 2.3).

$$\frac{p_2}{p_1} = e^{-(h_2-h_1)/H_e} \quad (10)$$

where:  $p_1$  and  $p_2$  is the atmospheric pressure at the heights  $h_1$  and  $h_2$ , respectively,  $H_e$  is pressure scale height

$$H_e = \frac{R_a T}{g} \quad (11)$$

$R_a$  – universal gas constant per unit mass,  $T$  temperature [K] and  $g$  – gravity.

The results of such an IPW RAOB – GPS comparison are presented in both versions (GPS meteo and RAOB meteo) for selected polar and subpolar stations in 2011 for EPN combined tropospheric product (Table 4). RAOB IPW bias depends on the radiosounding point – GNSS station distance and their latitude.

Table 3. Comparison of IPW from CIMEL Ittoqqortoormiit and GPS at Scoresbysund (SCOR) (differences: CIMEL – GPS); EPN tropospheric combination and IGS tropospheric product (hourly averages of 5 minute estimates)

Year	GPS solution	IPW average difference [mm]	Difference STD [mm]	Difference RMS [mm]	GPS estimates	CSPHOT measurements
2010	IGS	-0.16	0.48	0.51	647	1803
2011	IGS	0.08	0.49	0.49	312	777
2012	IGS	0.06	0.67	0.68	1262	4205
	EUR	0.07	0.71	0.71	1281	4281
2013	IGS	0.18	0.54	0.57	1036	3474
	EUR	0.22	0.50	0.54	1056	3538
2014	IGS	0.22	0.64	0.67	1128	3757
	EUR	0.25	0.50	0.56	1128	3757

Table 4. Comparison results of IPW from radiosoundings and GPS at selected stations (bias: RAOB – GPS); EPN combined tropospheric product (EUR) in 2011, for TIXI IGS solution; stations sorted by latitude

Radiosounding point	GPS	Distance [km]	Bias [mm]	Difference STD [mm]	Difference RMS [mm]	No of points
local meteo at GPS station						
4270 GL Narsarsuaq	QAQ1 43007M001	52.0	-0.10	1.55	1.55	715
4339 GL Ittoqqortoormi	SCOR 43006M002	9.7	0.27	0.73	0.78	594
4018 IS Keflavikurflug	REYK 10202M001	41.1	-0.18	1.18	1.19	691
3238 UK Albemarle	MORP 13299S001	26.4	-0.65	1.39	1.54	325
10113 DE Norderney	BORJ 14268M002	31.6	0.48	2.60	2.65	336
meteo from radiosounding						
4220 GL Aasiaat	KELY 43005M002	207.3	1.02	2.00	2.24	716
4270 GL Narsarsuaq	QAQ1 43007M001	52.0	-0.59	1.39	1.51	715
4339 GL Ittoqqortoormi	SCOR 43006M002	9.7	0.65	1.05	1.24	697
1004 NO NY-ALESUND II	NYA1 10317M003	3.4	0.49	0.82	0.95	385
1415 NO Stavanger	STAS 10330M001	24.2	0.57	1.44	1.55	666
1241 NO Orland	TRDS 10331M001	51.0	1.46	1.91	2.41	704
4018 IS Keflavikurflug	REYK 10202M001	41.1	1.60	1.47	2.17	690
2591 SN VISBY AEROLOG	VISO 10423M001	7.2	1.32	1.54	2.03	671
21824 RU Tiksi	TIXI 12319M001	15.0	1.92	1.79	2.62	694
3238 UK Albemarle	MORP 13299S001	26.4	-0.21	1.62	1.64	439
3913 UK Castor Bay	BELF 13240M001	32.7	0.95	1.49	1.77	532
10113 DE Norderney	BORJ 14268M002	31.6	0.50	2.55	2.60	353

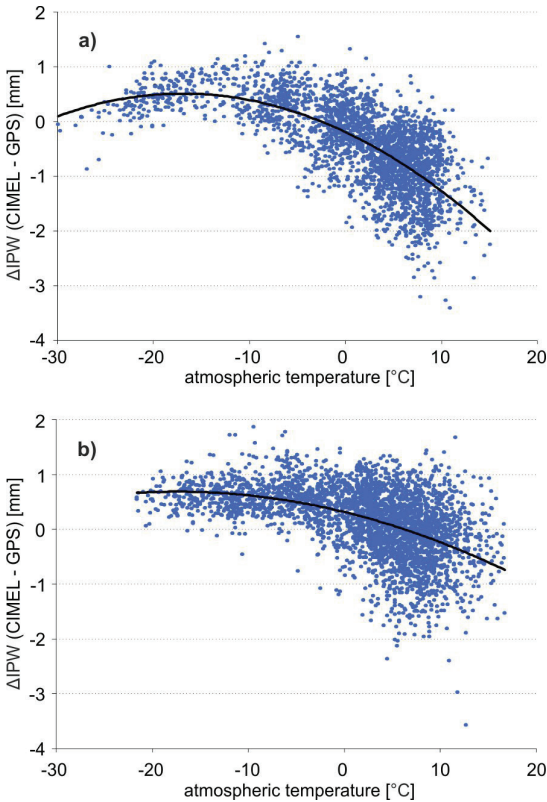


Fig. 11. IPW difference (CIMEL – GPS) for a) Thule-THU2 for 2009–2011, and b) Ittoqqortoormiit – Scoresbysund (SCOR) for 2012–2014 as function of atmospheric temperature, IGS tropospheric solution

Conformity of radiosounding and GPS derived IPW is of no surprise. Also for more distant stations (Narsarsuaq–Qaqortoq) quite good results with slightly greater dispersion were obtained (see Fig. 12).

There is no such seasonal periodicity (or temperature dependence) in IPW differences as in the case of CIMEL (Fig. 13). However, some periodicity of about 2 months can be observed in the series and needs further investigation.

Finally there is a possibility to directly compare aerological techniques, i.e. CIMEL sun-photometer and radiosoundings. The main problem here is a small number of common points: radiosoundings are performed only twice a day and only daily soundings at 12 UTC can be used. In the case of Ittoqqortoormiit in the period of 2010–2014 there are only 343 common points. Nevertheless IPW

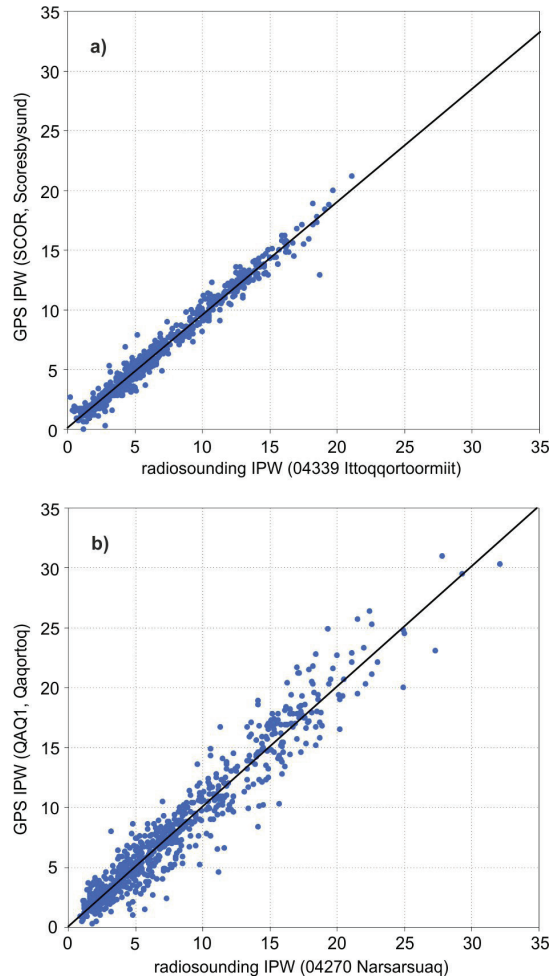


Fig. 12. IPW (RAOB vs. GPS) for a) Ittoqqortoormiit (04339 BGSC) – Scoresbysund (SCOR), and b) Narsarsuaq (04270 BGBW) – Qaqortoq (QAQ1) in 2012; distance in the first case is only 1 km, in the second: 62 km

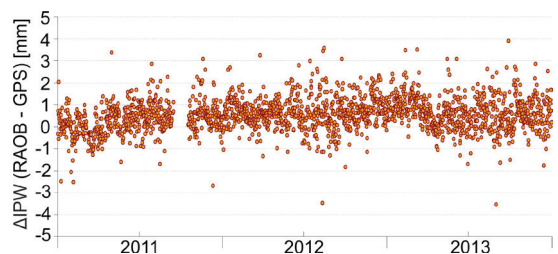


Fig. 13. IPW difference (RAOB – GPS) for Ittoqqortoormiit (04339 BGSC) – Scoresbysund (SCOR) IGS tropospheric solution, 2011–2013

difference once more exhibits temperature dependence (Fig. 14). The distance Ittoqqortoormiit – 04339 BGSC is only 600 m.

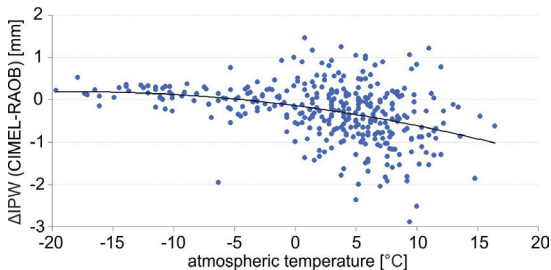


Fig. 14. IPW difference (CIMEL – RAOB) Ittoqqortoormiit – 04339 BGSC for 2010–2014 as a function of atmospheric temperature, IGS tropospheric solution

## Conclusions

IPW – this valuable meteorological parameter can be obtained both by classical aerologic techniques and derived from tropospheric solutions/products and treated as a reference to aerology. Three independent techniques have been tested to obtain Integrated Precipitable Water at four points in Greenland: GPS solution, radiosounding and CIMEL sunphotometer.

To calculate IPW for four GNSS stations, a local model of the mean temperature was developed using radiosoundings performed nearby by meteorological services. The linear formulae for mean temperature obtained in some cases considerably differ from the formulae obtained by Bevis et al. (2012) for stations in mid-latitudes because of the polar tropopause which is lower and relatively warmer in relation to the surface than tropopause for mid-latitudes.

CIMEL sunphotometer IPW and IPW values derived from standard solutions of IGS and EPN (combined solution) show relatively good agreement but also some biases of 2–7 %. IPW bias shows seasonal dependence (especially in the case of Thule), which signals some systematic deficiencies in solar photometry as an IPW retrieval technique. A probable cause of this phenomenon is a change in optical filter characteristics in sunphotometer working in extreme polar conditions.

Averaged IPW difference for RAOB – GPS is relatively small and show no dependence on temperature. The attempt to compare aerological techniques (CIMEL and RAOB) brings a similar temperature – IPW difference dependence but results are less pronounced.

In the polar environment with different sun visibility, GPS constellation geometry and temperature range, IPW series obtained by GPS and aerology show some characteristic discrepancies. There is empirical basis to claim that the GPS solution gives us at least as reliable results of IPW in the polar region as expert aerological techniques.

## Acknowledgements

This research was financially supported by the grant No. N N526 074038 of the Polish Ministry of Science and Higher Education/ National Science Centre. The author acknowledges the work of IGS staff, especially IGS tropospheric delay product developers: Yoaz Bar-Sever, Sung Byun and Sharyl Byram as well as EPN tropospheric product providers: Wolfgang Söhne and Rosa Pacione. Brent Holben (Goddard Space Flight Center NASA, principal investigator of AERONET instruments) and Alexander Smirnov (also GSFC) kindly agreed to my use of CIMEL data, and sent some valuable information and literature. Aleksander Pietruczuk (Institute of Geophysics, Polish Academy of Sciences) offered some interesting insights on CIMEL sunphotometer functioning. The author would like to thank Prof. Jan Kryński for his comments and suggestions indispensable for preparing the final version of the manuscript.

## References

- Alexandrov M.A., Schmid B., Turner D.D., Cairns B., Oinas V., Laciš A.A., Gutman S.I., Westwater E.R., Smirnov A., Eilers J., (2009): *Columnar water vapor retrievals from MFRSR data*, J. Geophys. Res., 114, D02306, doi:10.1029/2008JD010543.
- Andrews D.G., (2010): *An Introduction to Atmospheric Physics*, Second Edition, Cambridge University Press.
- Bevis M., Businger S., Herring T.A., Rocken Ch., Anthes R.A., Ware R.H., (1992): *GPS Meteorology' Remote Sensing of Atmospheric Water Vapor*

- Using the Global Positioning System*, J. Geophys. Res., Vol. 97, D14, pp. 15787–15801.
- Böhm J., Schuh H., (2013): *Atmospheric Effects in Space Geodesy*, Springer Heidelberg New York Dordrecht London, doi: 10.1007/978-3-642-36932-2.
- Byun S.H., Bar-Sever Y.E., (2009): *A new type of troposphere zenith path delay product of the international GNSS service*, J. Geod. (2009) 83: pp. 367–373, doi: 10.1007/s00190-008-0288-8.
- Davis J.L., Herring T.A., Shapiro I.I., Rogers A.E., Elgered G., (1985): *Geodesy by radio interferometry: Effects of atmospheric modelling errors on estimates of baseline length*, Radio Sci., 20, pp. 1593–1607 doi:10.1029/RS020i006p01593.
- Duan J., Bevis M., Fang P., Bock Y., Chiswell S., Businger S., Rocken C., Solheim F., Van Hove T., Ware R., McClusky S., Herring T.A., King R.W., (1996): *GPS meteorology: direct estimation of the absolute value of precipitable water*, J. Applied Met., 35, pp. 830–838. doi:10.1175/1520-0450.
- Halthore R.N., Eck T.F., Holben B.N., Markham B.L., (1997): *Sunphotometric Measurements of Atmospheric Water Vapor Column Abundance in the 940-nm Band*, J. Geophys. Res., 102, pp. 4343–4352.
- Holben B.N., Eck T.F., Slutsker I., Tanre D., Buis J.P., Setzer A., Vermote E., Reagan J.A., Kaufman Y.J., Nakajima T., Lavenue F., Jankowiak I., Smirnov A., (1998): *AERONET – A federated instrument network and data archive for aerosol characterization*, Rem. Sens. Env., 66(1), pp. 1–16.
- Holben B.N., Tanre D., Smirnov A., Eck T.F., Slutsker I., Abuhassan N., Newcomb W.W., Schafer J., Chatenet B., Lavenue F., Kaufman Y.J., Castle J.V., Setzer A., Markham B., Clark D., Frouin R., Halthore R., Karnieli A., O’Neill N.T., Pietras C., Pinker R.T., Voss K., Zibordi G., (2001): *An emerging ground-based aerosol climatology: Aerosol Optical Depth from AERONET*, J. Geophys. Res., 106, pp. 12067–12097.
- Hofmann-Wellenhof B., Lichtenegger H., Wasle E., (2008): *GNSS – Global Navigation Satellite Systems GPS, GLONASS, Galileo, and more*, Springer Wien New York.
- Kruczyk M., (2014): *Integrated Precipitable Water from GNSS as a climate parameter*, Geoinformation Issues, Vol. 6, No 1(6), pp. 21–35.
- Kruczyk M., Liwosz T., (2015): *Integrated precipitable water vapour measurements at Polish Polar Station Hornsund from GPS observations verified by aerological techniques*, Reports on Geodesy and Geoinformatics, Vol. 98, pp. 1–17; DOI: 10.2478/rgg-2015-0001.
- van Malderen R., Brenot H., Pottiaux E., Beirle S., Hermans C., De Mazière M., Wagner T., De Backer H., Bruyninx C., (2014): *A multi-site techniques intercomparison of integrated water vapour observations for climate change analysis*, Atmospheric Measurement Techniques Discussions, Vol. 7, Issue 2, pp. 1075–1151.
- Van der Marel H., (2004): *COST-716 demonstration project for the near real-time estimation of integrated water vapour from GPS*, Physics and Chemistry of the Earth, Parts A/B/C, 29, pp. 187–199.
- McIlven R., (2010): *Fundamentals of Weather and Climate*, Second Edition, Oxford University Press.
- Pacione R., Pace B., de Haan S., Vedel H., Lanotte R., Vespe F., (2011): *Combination Methods of Tropospheric Time Series*, Adv. Space Res., 47(2), pp. 323–335, doi: 10.1016/j.asr.2010.07.021.
- Rocken C., Ware R., van Hove T., Solheim F., Alber C., Johnson J., Bevis M., Businger S., (1993): *Sensing atmospheric water vapor with the Global Positioning System*, Geophys. Res. Lett., 20, 2631.
- Saastamoinen J., (1972): *Atmospheric Correction for the troposphere and stratosphere in radio ranging of satellites*, The Use of Artificial Satellites for Geodesy Geophysics Monograph Series, (ed.) S.W. Henriksen et al., pp. 247–251.
- Salby M.L., (2012): *Physics of the Atmosphere and Climate*, Cambridge University Press.
- Shelton M.L., (2009): *Hydrometeorology. Perspectives and Applications*, Cambridge University Press.
- Schmid B., Michalsky J.J., Slater D.W., Barnard J.C., Halthore R.N., Liljegren J.C., Holben B.N., Eck T.F., Livingston J.M., Russell P.B., Ingold T., Slutsker I., (2001): *Comparison of columnar water-vapour measurements from solar transmittance methods*, Applied Optics, Vol. 40, No 12, pp. 1886–1896.
- Söhne W., Weber G., (2009): *Status Report of the EPN Special Project “Troposphere Parameter Estimation”*, EUREF Publication No 15 Mitteilungen des Bundesamtes für Kartographie und Geodäsie 42(15), pp. 79–82.
- Vazquez G.E., Brzezinska D., (2012): *GPS-PWV estimation and validation with radiosonde*

*data and numerical weather prediction model in Antarctica*, GPS Solutions, doi:10.1007/s10291-012-0258-8.

Vedel H., Mogensen K.S., Huang X.-Y., (2001): *Calculation of zenith delays from meteorological data, comparison of NWP model, radiosonde and GPS delays*, Phys. Chem. Earth, Vol. 26, No 6–8, pp. 497–502.

### WWW References

AERONET data: [http://aeronet.gsfc.nasa.gov/data\\_menu.html](http://aeronet.gsfc.nasa.gov/data_menu.html)

Radiosonde ZPD biases (EPN): [http://www.epncb.oma.be/\\_networkdata/radiosonde\\_zpd\\_biases.php](http://www.epncb.oma.be/_networkdata/radiosonde_zpd_biases.php)

Mean temperature data (TU Wien): <http://ggosatm.hg.tuwien.ac.at/DELAY/ETC/TMEAN>

## Porównanie technik pomiarów kolumnowej zawartości pary wodnej w obszarze polarnym

Michał Kruczyk

Katedra Geodezji i Astronomii Geodezyjnej, Politechnika Warszawska

Pl. Politechniki 1, 00-661, Warszawa

Tel/Fax: +48 22 2347754, E-mail: [kruczyk@gik.pw.edu.pl](mailto:kruczyk@gik.pw.edu.pl)

**Streszczenie:** Rozwiązania troposferyczne IGS i EPN zostały wykorzystane do przetestowania dwu technik pomiarów aerologicznych dla stacji GNSS w regionie polarnym (Grenlandia). Parametr meteorologiczny jakim jest scałkowana zawartość pary wodnej (IPW) został pozyskany za pomocą standardowej procedury opisanej w literaturze. Do przeliczania IPW z wilgotnej części opóźnienia opracowano lokalny model temperatury średniej (zależność linowa względem temperatury na wysokości 2 metrów nad powierzchnią ziemi) wyznaczony z radiosondowań prowadzonych w sąsiedztwie stacji GNSS. Pomiaru fotometryczne udostępnia sieć pomiarów aerozoli AERONET działająca pod egidą NASA. Porównania kilkuletnich szeregów IPW wykazują systematyczne różnice między IPW z GNSS a fotometrem słonecznym (ale nie radiosondażem). IPW z fotometru jest nie tylko średnio kilka procent mniejsza niż z GNSS ale różnica ta zmienia się wraz z porami roku i temperaturą (co jest szczególnie widoczne w warunkach polarnych). To wykazuje pewien istotny problem z fotometrią słoneczną jako techniką pomiarów kolumnowej pary wodnej. Fotometr wykazuje systematyczną różnicę IPW (zależną od temperatury atmosferycznej) także w stosunku do wyników radiosondażu.

**Słowa kluczowe:** para wodna, meteorologia GNSS, kolumnowa (scałkowana) zawartość pary wodnej, fotometr słoneczny, radiosondaż, badania polarne, Grenlandia



# Application of NOAA AVHRR satellite images for studying various environmental and climatic conditions in Polish forests

---

Zbigniew Bochenek

Institute of Geodesy and Cartography, 27 Modzelewskiego St., 02-679, Warsaw, Poland  
Tel.: +48 22 3291977, Fax: +48 22 3291950, E-mail: zbigniew.bochenek@igik.edu.pl

Dariusz Ziółkowski

Institute of Geodesy and Cartography, 27 Modzelewskiego St., 02-679, Warsaw, Poland  
Tel.: +48 22 3291991, Fax: +48 22 3291950, E-mail: dariusz.ziolkowski@igik.edu.pl

Maciej Bartold

University of Warsaw, Faculty of Geography and Regional Studies, Department of Geoinformatics, Cartography and Remote Sensing

Institute of Geodesy and Cartography, 27 Modzelewskiego St., 02-679, Warsaw, Poland  
Tel.: +48 22 3291978, Fax: +48 22 3291950, E-mail: maciej.bartold@igik.edu.pl

**Abstract:** The main objective of the presented work is to make an evaluation of the applicability of low-resolution satellite data for studying the condition of Polish forests being under impact of various climatic and environmental factors. NOAA AVHRR images were used in the work; vegetation indices derived from these images were combined with meteorological parameters obtained from weather stations. Six forest study areas representing different climatic and environmental conditions were used in the research work. The results of the study revealed that there are statistical relationships between remote sensing based indices derived for forest areas from low-resolution satellite data and temperature information characterizing climatic conditions, especially in the first part of the growing season. These findings were confirmed both in the spatial context – in various climatic zones – and in the temporal context.

**Keywords:** climate change, forest monitoring, low-resolution satellite data, vegetation index

---

*Received: 17 December 2015 / Accepted: 23 April 2016*

## 1. Introduction

Forests are one of the most important terrestrial ecosystems; it is recognized that they can respond to climate changes and natural / man made disturbances in a non-linear way (Lambin et al., 1997). The impact of disturbance factors is region / site dependent, hence there is a need to investigate this problem in the regional scale. Monitoring of the impact of climate changes on vegetation development with the use of remote sensing has been reported in recent publications (Stow et al., 2004; Lhermitte et al., 2011; Li et al., 2013; Hawinkel et al., 2015; Krishnan et al., 2015; de Moura et al., 2015). Most often the authors used for monitoring purposes Normalized Difference Vegetation Index

(NDVI), widely recognized as an indicator of vegetation condition. Multi-scale satellite images have been used for research work, starting from high-resolution images (Landsat type) down to low-resolution satellite data (MODIS, NOAA AVHRR, SPOT Vegetation) (Jepsen et al., 2009; Bokhorst et al., 2012; Ivits et al., 2012; Griffiths et al., 2014; Hermosilla et al., 2015). Various approaches to analysis of time series based on satellite derived indices were applied, in order to derive proper information on their usefulness for climate change monitoring, including time series segmentation (Jamali et al., 2015).

The goal of the presented work is to evaluate the usefulness of low-resolution NOAA AVHRR data for monitoring Polish forests representing various

environmental and climatic conditions. In order to achieve the goal of the research work a detailed spatial and temporal analysis of meteorological parameters was carried out in combination with spatial and temporal variability of vegetation indices derived from satellite images. Two vegetation indices – NDVI and VCI (Vegetation Condition Index) – were analysed in conjunction with a meteorological database, containing temperature and precipitation data, using a statistical method of regression analysis. The outcome from statistical analysis reveals good relationships between remote sensing based and meteorological parameters, thus enabling the authors to draw conclusions on stress conditions in Polish forests.

## 2. Study area

In order to cover various environmental conditions in Poland six forest study areas were selected for the research work. Four forest areas – Augustowska Forest, Białowieska Forest, Knyszynska Forest and Borecka Forest – are located in northeastern

Poland. This part of Poland is under the influence of a continental climate, characterized by the impact of polar air masses, a shorter vegetation period and large temperature fluctuations. The four forest areas differ in forest site characteristics of species compositions: Augustowska and Knyszynska forests represent mainly coniferous forests (pine and spruce stands), while Białowieska and Borecka Forests include large areas of deciduous and mixed stands (with hornbeam, oak, alder and birch as the main species).

Two other study areas are located in southern and southwestern Poland. Forests in Beskid Żywiecki Mountains are situated in the zone of continental climate zone with the impact of the tropical zone, while forests in Karkonosze Mountains belong to the zone of maritime climate zone with the impact of tropical air masses. Both southern study areas are located in mountainous regions, with two dominant species – spruce and beech.

The location of all study areas is presented in Figure 1.

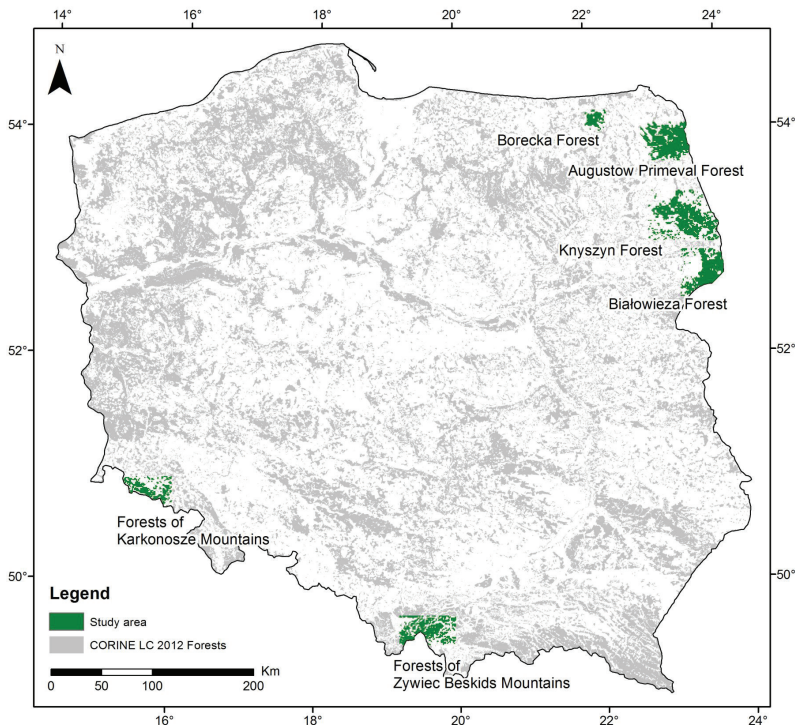


Fig. 1. Location of forest study areas

### 3. Materials and methods

1-km NOAA AVHRR images were used as the basic material for the research work. The images collected by a receiving station installed at the Institute of Geodesy and Cartography, Warsaw, Poland were pre-processed geometrically and radiometrically, including an atmospheric correction algorithm; next a cloud screening procedure was conducted applying the split-window technique and individual images were composited to produce 10-day cloud-free composites. Next values of two vegetation indices – Normalized Difference Vegetation Index (NDVI) and Vegetation Condition Index (VCI) – were extracted from the regions of interest: six forest areas located in southern, southwestern and northeastern Poland. The values were collected both for the whole forest areas and for 1-km test sites representing homogeneous tree stands.

At the next stage of the work NDVI time series were generated for each study area, covering the vegetation period (April – September) for the dataset comprising NDVI images from 1997 to 2015. Preliminary analysis of these series revealed a problem of quite high fluctuation of NDVI values within the vegetation period, which had to be analysed and accounted for prior to the next stage of the work – comparison of changes of remote sensing based indices with changes of meteorological parameters for the study areas. Therefore, two approaches of smoothing NDVI time series were applied in order to remove noise existing in original values due to non-precise cloud removal and changeable atmospheric conditions – a method of noise reduction based on the Savitzky-Golay filter (Bojanowski et al., 2009) and a method applying the spline technique. Moreover, in order to reduce fluctuations of NDVI values the study was conducted with the use of parameters describing short-term changes in atmosphere (temperature and humidity). The first results of the study revealed, that there is a relation between major changes in the atmosphere and abrupt NDVI decline. As a result of that study it was found that the smoothing method based on the Savitzky-Golay filter renders more precisely the NDVI run within the vegetation period, preserving subtle changes and removing abnormal ones.

The research was also conducted to determine whether NDVI values derived from low-resolution

satellite images for the large forest areas, which include mixed forest information (e.g. deforestation patches, boundary mixed pixels, etc.) can be representative for dominant tree stands. The study included a comparison of the vegetation index derived from:

- the forest mask which encompassed the whole forest study area, as defined by CORINE Land Cover map, assuming that boundary pixels which include more than 50 % of forest belong to the forest mask,
- 1-km homogeneous test sites distributed with the forest study area as a mean NDVI value obtained from 8–12 sites.

The analysis was carried out for all six study areas located in northeastern and southern Poland. The results of the study proved that NDVI values derived for forest masks are compatible with means from 1-km test sites, whereas individual test sites can slightly deviate from that pattern. Compatibility of both NDVI curves, derived from 1-km test sites and from the whole forest polygons, is presented in Figure 2, using as an example the Borecka Forest test site.

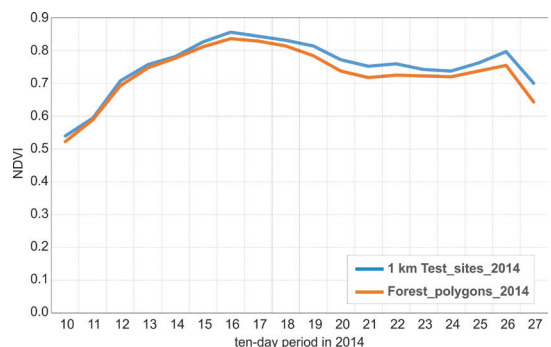


Fig. 2. Comparison of NDVI curves derived from eight 1-km test sites and from the whole forest area

At the next stage meteorological data were compiled from weather stations adjoining study areas: air temperature and precipitation (including information on snow appearance). These data were analysed in order to find anomalous weather periods, which could affect the condition of tree stands within study areas. As a result of the analysis three years which differ greatly in meteorological condi-

tions were selected for comparative analysis – 2006, 2013 and 2014. The year 2014 was characterized by a mild winter, with temperatures above 0 from mid-February, reaching a maximum temperature at the beginning of August and gradually decreasing until the end of October. There were three precipitation peaks within the vegetation period – in ten-day periods 14, 19–20 and 23. In contrast, in 2006 and 2013 winters were quite long – with the air temperature below 0 until the beginning of April and with snow coverage, followed by a rapid temperature increase to the end of July / beginning of August. In 2013 there were three precipitation peaks within vegetation period – in ten-day periods 15, 16, 20 and 26, while there were two in 2006 – in ten-day periods 15 and 23. The graph demonstrating air temperature changes for northeastern forests in 2006, 2013 and 2014 is presented in Figure 3.

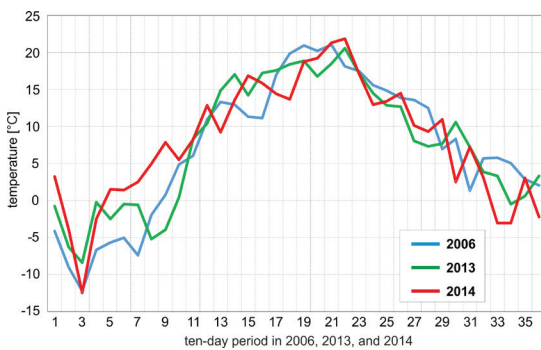


Fig. 3. Air temperature changes for northeastern forests in 2006, 2013 and 2014

#### 4. Results and discussion

At the next stage of the works NDVI indices derived from NOAA AVHRR data collected in the 2000 – 2015 period were computed for forests located in six study areas: four in northeastern Poland – Białowiecka Forest, Knyszynska Forest, Augustowska Forest, Borecka Forest – and two located in southern Poland – Beskid Zywiecki and Karkonosze. The thorough analysis of NDVI curves was performed in two aspects:

- in the spatial context,
- in the temporal context.

Analysis of NDVI runs for study areas located in various geographical regions in northeastern and in southern Poland revealed quite important differences, caused both by different climatic conditions and environmental aspects. In the case of high temperatures at the end of winter and beginning of spring (2014) NDVI for forest study areas located in southern Poland begins from lower values due to the later start of the growing season in the Beskid and Karkonosze mountains. It is next compensated by favourable temperature conditions, reaching in ten-day periods 15–16 (May – June) similar values to the remaining forest areas. Forests in mountainous regions are more sensitive to NDVI fluctuations due to more variable climatic conditions. The lowest NDVI values in the mid-growing season are observed for Augustowska and Knyszynska Forests, which are the study areas more influenced by the continental climate than the remaining ones. NDVI changes for all study areas in 2014 are presented in Figure 4.

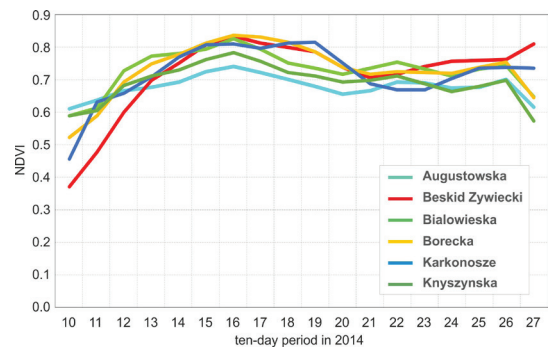


Fig. 4. NOAA NDVI changes for all forest study areas in 2014

A different situation of NDVI runs is observed in the case of the “cold” year, represented by low temperatures at the end of winter / beginning of spring (2006). In this case NDVI values for all study areas are low at the beginning of the growing season (the lowest one for the Karkonosze test site), reaching quite similar values in the mid-growing season. In the second part of the growing season – ten-day periods 20–27 (July – September) – test areas represented predominantly by mixed forests (Białowiecka and Borecka Forests) reveal higher NDVI values than the remaining ones. Again, lower

NDVI values can be observed for Augustowska and Knyszynska Forests, influenced by a more continental climate. NDVI changes for all study areas in 2006 are presented in Figure 5.

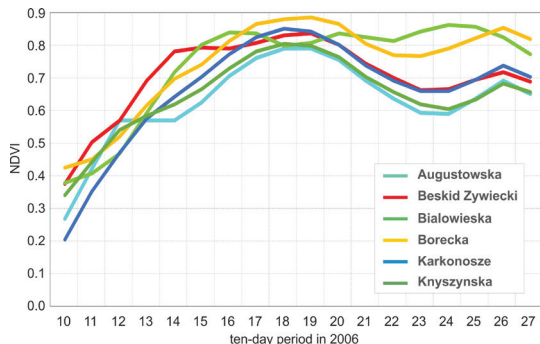


Fig. 5. NOAA NDVI changes for all forest study areas in 2006

Analogous analysis was conducted in the temporal aspect. NDVI curves were compared for particular forest test sites in the consecutive years 2000 – 2015. Analysis of the variability of NDVI values throughout the growing season revealed quite important differences, depending on the year represented by specific meteorological conditions. Three years representing different meteorological conditions at the beginning of growing season – 2006 and 2013 characterized by low temperatures at the end of winter / beginning of spring and 2014 when the growing season was preceded by a mild winter (temperatures in March above 0°C) – were selected for illustration purposes. Analysis of NDVI in these years for northeastern forests revealed low values at the beginning of the growing season 2006 and 2013, as compared to 2014, for all three forest areas. Lower NDVI values existed until ten-day periods 15–16 (end of May / beginning of June); they also appeared in the case of 2013 at the end of the growing season. Comparison of NDVI changes for northeastern forests is presented in Figures 6 and 7.

In order to support analysis of NDVI changes an additional parameter characterizing the forest condition – Vegetation Condition Index (VCI) – was also applied. VCI is based on present and historical values of NDVI; it is expressed by the formula:

$$VCI = (NDVI_i - NDVI_{min}) / (NDVI_{max} - NDVI_{min})$$

where  $NDVI_i$  means NDVI value in the  $i$  ten-day period,  $NDVI_{max}$  and  $NDVI_{min}$  are the maximum value of NDVI and the minimum value of NDVI in the historical database, respectively.

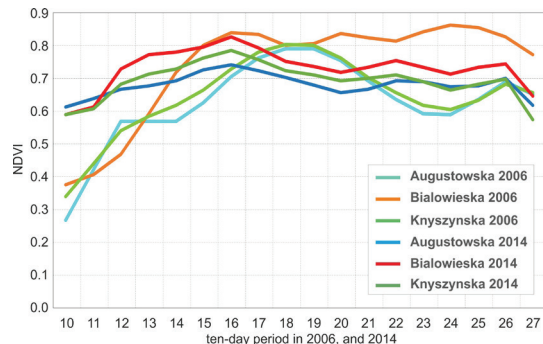


Fig. 6. Comparison of NDVI changes for northeastern forests – 2006 and 2014

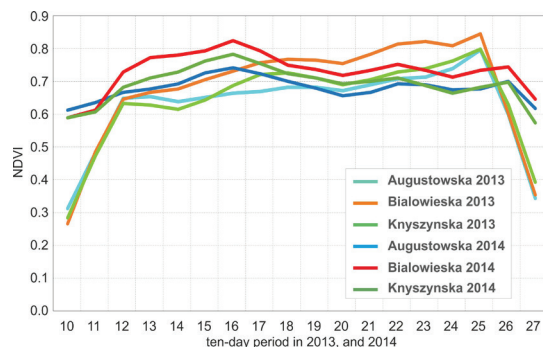


Fig. 7. Comparison of NDVI changes for northeastern forests – 2013 and 2014

The Vegetation Condition Index has been computed for all years in the 2000 – 2015 period and for all forest study areas. The results of analysis of VCI curves support those obtained from NDVI analysis – in the first part of vegetation seasons 2006 and 2013 (until ten-day period 17 – mid-June) VCI values were much lower than those observed in 2014. A comparison of VCI changes for northeastern forests is presented in Figures 8 and 9.

As thorough comparison of NDVI and VCI curves pointed out that there are some relationships between the character of meteorological conditions and values of vegetation indices, at the next stage of the works the quantitative assessment of these relations was conducted, through statistical analysis of remote

sensing based and meteorological datasets. Various parameters derived from these datasets were applied:

- mean temperature for the winter period (January – March);
- mean temperature in March;
- mean temperature in the third ten-day period of March;
- NDVI / VCI value in the first ten-day period of April;
- NDVI / VCI value representing curve in the first six ten-day periods (April – May);
- NDVI / VCI value representing curve in the whole growing season.

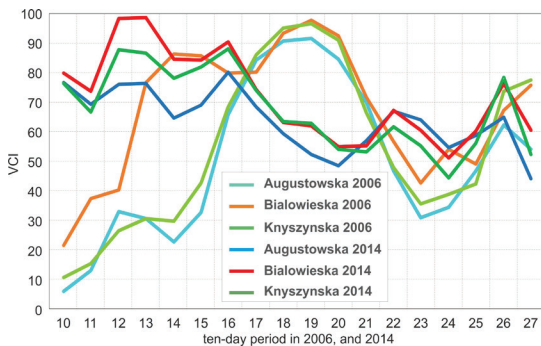


Fig. 8. Comparison of VCI changes for northeastern forests – 2006 and 2014

It was assumed that air temperature in winter-time and at the beginning of the growing season can have a significant impact on vegetation development, as expressed by vegetation indices. The de-

tailed correlation analysis between temperatures and NDVI / VCI indices revealed that there is quite a strong correlation between mean air temperature in March and value of NDVI, represented by the area under the NDVI curve in the first six ten-day periods of the growing season. A high correlation coefficient appears for 5 study areas (except the Beskid Zywiecki test site). These findings are confirmed by correlation analysis between mean air temperature in March and the Vegetation Condition Index.

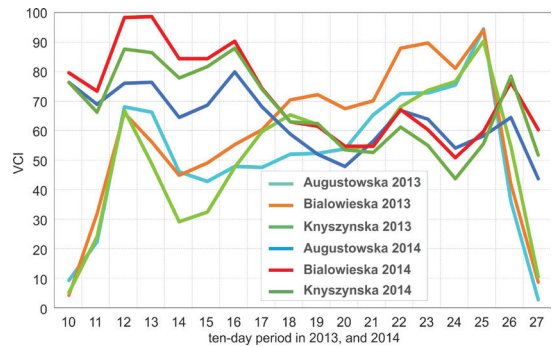


Fig. 9. Comparison of VCI changes for northeastern forests – 2013 and 2014

Slightly lower correlations were obtained between mean air temperature in the third ten-day period of March and the sum of vegetation indices in the first six ten-day periods, whereas correlations between mean winter temperature and the sum of NDVI / VCI are not so evident (exist only for some forest areas).

Table 1. Results of correlation analysis between air temperatures and NDVI / VCI derived from the first six ten-day periods of the growing season

Name of test area	Winter		March		March 3 <sup>rd</sup> ten-day period	
	NDVI	VCI	NDVI	VCI	NDVI	VCI
Augustowska Forest	<b>0.51</b>	<b>0.55</b>	<b>0.64</b>	<b>0.67</b>	<b>0.50</b>	0.47
Białowiecka Forest	0.39	0.28	<b>0.63</b>	<b>0.53</b>	<b>0.53</b>	0.42
Knyszynska Forest	0.45	0.44	<b>0.66</b>	<b>0.50</b>	<b>0.58</b>	0.32
Borecka Forest	<b>0.64</b>	<b>0.73</b>	<b>0.86</b>	<b>0.87</b>	<b>0.51</b>	0.45
Beskid Zywiecki	0.13	0.31	0.30	0.45	0.14	0.16
Karkonosze	<b>0.61</b>	<b>0.50</b>	<b>0.67</b>	0.49	0.32	0.16

Significant correlation was not found between air temperatures and NDVI values derived from the area under the NDVI curve in the whole vegetation period.

In the case of relationships between air temperatures in wintertime / March / end of March and NDVI / VCI in the tenth ten-day period (first ten-day period of the growing season) these correlations were somewhat lower compared to previous ones, but still exist, especially in the arrangement NDVI / VCI versus air temperature in the third ten-day period of March.

There are some differences in correlation coefficients between particular forest areas; the highest coefficients were obtained for Borecka Forest ( $r = 0.87$ ), while the lowest for Beskid Zywiecki ( $r = 0.30$ ). Results of the correlation analysis are presented in Table 1 and in Figure 10.

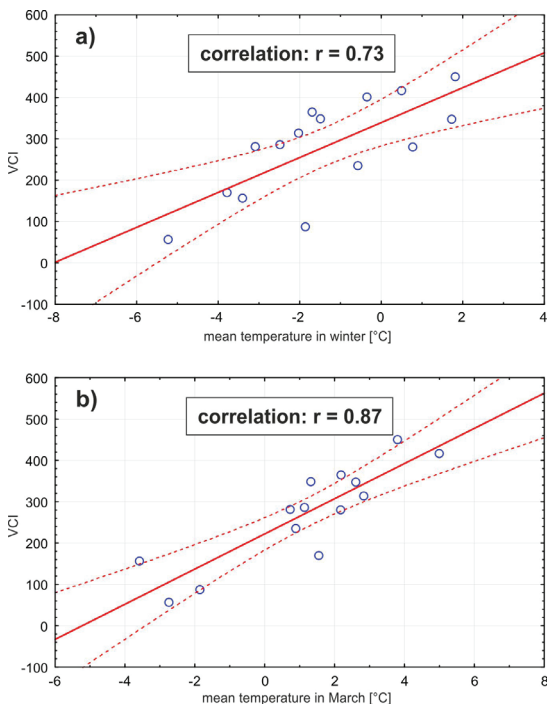


Fig. 10. Correlation graphs: a) for mean temperature in winter, b) for mean temperature in March (Borecka Forest)

## 5. Conclusions

The aim of the presented work was to evaluate the applicability of low-resolution satellite data for

studying various environmental and climatic conditions in Polish forests. The results of the work revealed that both aspects of forest variability can be to a large extent monitored with the use of vegetation indices derived from NOAA AVHRR images. Forest areas located in various climatic regions – under the impact of continental climate in north-eastern Poland and under the impact of the maritime climate in southwestern Poland are characterized by different NDVI curves, especially at the beginning and end of the growing season. General species composition within the study areas – dominance of coniferous or deciduous / mixed forests – also has a visible impact of NDVI levels.

Study of relationships between meteorological parameters and vegetation indices derived from NOAA AVHRR images also led to the conclusion that there is quite a significant relation between these two types of data. Both indices – Normalized Difference Vegetation Index (NDVI) and Vegetation Condition Index (VCI) – derived from the first part of the vegetation season correlate well with temperatures existing in wintertime, especially at the end of winter (in March). It means that low-resolution satellite data can be applied for monitoring stress conditions at the beginning of the growing season. Nevertheless, it should be mentioned that a significant impact of unfavourable conditions expressed by low winter / early spring temperatures is not observed for the study areas, while analysing vegetation indices in the whole growing season. It implies the conclusion that Polish forests located in both climatic zones are quite resistant to anomalies of temperature at the onset of the vegetation season.

The results of this study indicate further research which will be based on high-resolution satellite data; these data will enable more detailed analysis of relations between climatic conditions, environmental aspects and indices derived from EO images, taking into account variability of species and sites within the study areas.

## Acknowledgments

The research work was conducted within the Polish-Norwegian Research Programme, Norway Grants, financed by the National Centre for Research and

Development, as a part of the WICLAP project “Ecosystem stress from the combined effects of winter climate change and air pollution – how do the impacts differ between biomes?”

## References

- Bojanowski J., Kowalik W., Bochenek Z., (2009): *Noise reduction of NDVI time-series: a robust method based on Savitzky-Golay filter*, Annals of Geomatics 2009, Vol. VII, No 2(32), pp. 13–21.
- Bokhorst S., Tømmervik H., Callaghan T., Phoenix G., Bjerke J.W., (2012): *Vegetation recovery following extreme winter warming events in the sub-Artic estimated using NDVI from remote sensing and handheld passive proximal sensors*, Environmental and Experimental Botany 81, pp. 18–25.
- Griffiths P., Kuemmerle T., Baumann M., Radeloff V.C., Abrudan I.V., Lieskovsky J., Munteanu C., Ostapowicz K., Hostert P., (2014): *Forest disturbances, forest recovery, and changes in forest types across the Carpathian ecoregion from 1985 to 2010 based on Landsat image composites*, Rem. Sens. of Environment, Vol. 151, pp. 72–88.
- Hawinkel P., Swinnen E., Lhermitte S., Verbist B., Van Orshoven J., Muys B., (2015): *A time series processing tool to extract climate-driven inter-annual vegetation dynamics using Ensemble Empirical Mode Decomposition (EEMD)*, Rem. Sens. of Environment, Vol. 169, pp. 375–389.
- Hermosilla T., Wulder M.A., White J.C., Coops N.C., Hobart G.W., (2015): *Regional detection, characterization, and attribution of annual forest change from 1984 to 2012 using Landsat-derived time-series metrics*, Rem.Sens. of Environment, Vol. 170, pp. 121–132.
- Ivits E., Cherlet M., Tóth G., Sommer S., Mehl W., Voght J., Micale F., (2012): *Combining satellite derived phenology with climate data for climate change impact assessment*, Global and Planetary Change 88-89, pp. 85–97.
- Jamali S., Jönsson P., Eklundh L., Ardö J., Seaquist J., (2015): *Detecting changes in vegetation trends using time series segmentation*, Rem. Sens. of Environment, Vol. 156, pp. 182–195.
- Jepsen J.U., Hagen S.B., Høgda K.A., Ims R.A., Karlsen S.R., Tømmervik H., Yoccoz N.G., (2009): *Monitoring the spatio-temporal dynamic of geometric moth outbreaks in birch forest using MODIS-NDVI data*, Rem. Sens. of Environment, Vol. 113, pp. 1939–1947.
- Krishnan P., Kochendorfer J., Dumas E.J., Guillevic P.C., Baker C.B., Meyers T.P., Martos B., (2015): *Comparison of in-situ, aircraft, and satellite land surface temperature measurements over a NOAA Climate Reference Network site*, Rem. Sens. of Environment, Vol. 165, pp. 249–264.
- Lambin E.F., Ehrlich D., (1997): *Land cover changes in sub-Saharan Africa (1982–1991): Application of a change index based on remotely sensed surface temperature and vegetation indices at a continental scale*, Rem. Sens. of Environment, Vol. 61, pp. 181–200.
- Lhermitte J., Verbesselt W., Verstraeten W., Coppin P., (2011): *A comparison of time series similarity measures for classification and change detection of ecosystem dynamics*, Rem. Sens. of Environment, Vol. 115, Issue 12, pp. 3129–3152.
- Li Z., Huffman T., McConkey B., Townley-Smith L., (2013): *Monitoring and modeling spatial and temporal patterns of grassland dynamics using time-series MODIS NDVI with climate and stocking data*, Rem. Sens. of Environment, Vol 138, pp. 232–244.
- de Moura Y.M., Hilker T., Lyapustin A., Galvão L.S., dos Santos J.R., Anderson L.O., de Sousa C.H.R., Arai E., (2015): *Seasonality and drought effects of Amazonian forests observed from multi-angle satellite data*, Rem. Sens. of Environment, Vol. 171, pp. 278–290.
- Stow D.A., Hope A., McGuire D., Verbyla D., Gamon J., Huemmrich F., Houston S., Racine C., Sturm M., Tape K., Hinzman L., Yoshikawa K., Tweedie C., Noyle B., Silapaswan C., Douglas D., Griffith B., Jia G., Epstein H., Walker D., Daeschner S., et al. (2004): *Remote sensing of vegetation and land-cover change in Arctic Tundra Ecosystems*, Rem. Sens. of Environment, Vol. 89, Issue 3, pp. 281–308.

## Zastosowanie obrazów satelitarnych NOAA AVHRR do badania warunków środowiskowych i klimatycznych w polskich lasach

Zbigniew Bochenek

Institut Geodezji i Kartografii, ul. Modzelewskiego 27, PL 02-679 Warszawa  
Tel.: +48 22 3291977, Fax: +48 22 3291950, E-mail: zbigniew.bochenek@igik.edu.pl

Dariusz Ziółkowski

Institut Geodezji i Kartografii, ul. Modzelewskiego 27, PL 02-679 Warszawa  
Tel.: +48 22 3291991, Fax: +48 22 3291950, E-mail: dariusz.ziolkowski@igik.edu.pl

Maciej Bartold

Uniwersytet Warszawski, Wydział Geografii i Studiów Regionalnych, Zakład Geoinformatyki, Kartografii  
i Teledetekcji

Institut Geodezji i Kartografii, ul. Modzelewskiego 27, PL 02-679 Warszawa  
Tel.: +48 22 3291978, Fax: +48 22 3291950, E-mail: maciej.bartold@igik.edu.pl

**Streszczenie:** Głównym celem prezentowanej pracy jest ocena możliwości wykorzystania niskorozdzielczych obrazów satelitarnych do badania kondycji drzewostanów w polskich lasach, będących pod wpływem różnych czynników klimatycznych i środowiskowych. W pracy zostały wykorzystane obrazy satelitarne NOAA AVHRR; wskaźniki roślinności określone na podstawie tych obrazów zostały porównane z parametrami meteorologicznymi otrzymanymi z naziemnych stacji pogodowych. Badania przeprowadzono dla 6 obszarów leśnych reprezentujących różne warunki klimatyczne i środowiskowe. Wyniki prac wykazały, iż istnieją statystyczne zależności pomiędzy wskaźnikami roślinności określanymi na podstawie niskorozdzielczych obrazów satelitarnych a temperaturą powietrza charakteryzującą warunki klimatyczne, zwłaszcza w pierwszej części okresu wegetacyjnego. Wnioski te zostały potwierdzone w aspekcie przestrzennym – w różnych strefach klimatycznych oraz w aspekcie czasowym.

**Słowa kluczowe:** zmiany klimatyczne, monitoring lasów, niskorozdzielcze obrazy satelitarne, wskaźnik roślinności



# Automated measuring devices for pendulum wire displacements

---

Mieczysław Kołodziejczyk

Institute of Geodesy and Cartography, 27 Modzelewskiego St., 02-679 Warsaw, Poland

Tel.: +48 22 3291912, Fax.: +48 22 3291950 E-mail: mieczyslaw.kolodziejczyk@igik.edu.pl

**Abstract:** The article describes the construction and principle of operation of two prototype devices: a laser device and an inductive device for measuring the pendulum wire displacement. A rotating laser beam and two inside detectors (fixed), as well as two external detectors were used in the first device. Falling on the detectors, the laser beam will cause them to generate electrical signals. The time differences between the signals generated by the internal (fixed) and external detectors are a function of the pendulum wire displacement. Inductive sensors mounted inside the measuring head, which is fixed to a cross-truck, moving along the perpendicular  $X$  and  $Y$  axes in the range of 50 mm, were used in the second device. The cross-truck is moved by stepper motors, and the inductive sensors placed in the  $X$  and  $Y$  axes search for the location of the pendulum wire. The number of steps of the stepper motors is a measure of the pendulum wire displacement along the  $X$  and  $Y$  axes.

Such devices are used to control the deviation of verticality of tall hydro-technical facilities mainly due to the action of internal stresses and external factors such as temperature and the water level in the tank.

**Keywords:** deviation of verticality, measurement of displacement, pendulum, pendulum wire, hydro-technical facilities

---

*Received: 9 March 2016 / Accepted: 18 April 2016*

## 1. Introduction

Tall structures are deviated from verticality mainly due to the action of internal stresses and external factors (Brys, 2000). On account of the safety of such structures, in particular hydro-technical ones, it is necessary to systematically monitor and measure deformations in accordance with a schedule of measurements (Brys, 2000; Janusz and Janusz, 2004). Inclinometers and pendulums are used for measuring inclinations of structures. A pendulum consists of a wire mounted at the highest possible point of a structure and a weight submerged in a tank with oil, and fixed at the lowest possible point of this structure. Placing the weight in the oil tank serves the purpose of damping the pendulum wire vibrations, thus increasing the accuracy of measurement. Inverse pendulums, in which the wire is mounted at the lower part of a structure, with the oil tank and the float fixed high in the upper part, are also used. Measurements of the pendulum wire displacement are performed manually, or in

automated measurement systems, and consist in measuring changes to the position of the wire against a set of reference planes.

In many structures, due to difficult environmental conditions, measurements of pendulum wire displacements are performed only using manual optomechanical instruments (Janusz et al., 1974). Such measurements are time-consuming and, therefore, are performed not more than a few times a year. There are also structures on which automated measuring systems recording changes in various parameters affecting the security of a structure are installed; such systems in many cases do not, however, record changes to the position of the pendulum wire (Smolka, 1994).

It was in the Institute of Geodesy and Cartography, in cooperation with OLBRYSZ ELECTRONIC company, that prototypes of devices for measuring the pendulum wire displacement, which can be used on almost all tall hydro-technical structures, were developed and constructed. These devices can be installed on tested structures and connected

to the automated systems of measuring displacements and deformations functioning there, without interrupting the continuity of measurements carried out using manual instruments. Due to the severe conditions in which a device measuring the pendulum wire displacement operates, the development of such a device is a very difficult matter.

However, efforts have been made to develop the construction of such a device. The results of this work include prototypes, publications (Mirek, 2003) and patents (Cmielewski, 2003; Ohtomo Fumio, 2003; Bryś and Cmielewski, 2004; Kołodziejczyk and Olbrysz, 2007).

## 2. Description of the devices

The first device implementing the measurement of pendulum wire displacements, designed and constructed at the Institute of Geodesy and Cartography, is a laser device (Kołodziejczyk and Olbrysz, 2007). The principle of operation of this device is presented in Figure 1. This device consists of a laser light source, a rotating mirror, two tag detectors and two receiving detectors. These elements are enclosed in a shared sealed housing, which is partly opened for the time of conducting measurements, and then closed after their completion. The beam emitted by the laser light source is reflected from the rotating mirror, creating a rotating beam which, falling on the tag detectors, causes them to generate electrical impulses. At the same time, the beam reflected from the pendulum wire falls onto the receiving detectors, which also induce electrical impulses. The time dif-

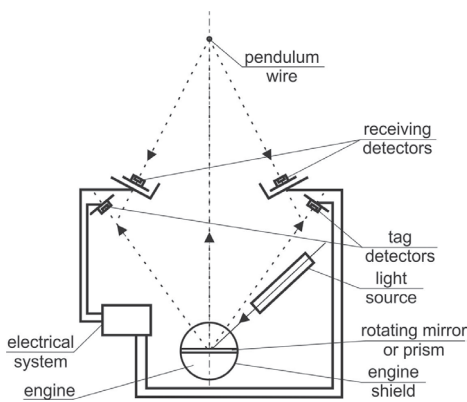


Fig. 1. A diagram of a laser device for measuring pendulum wire displacements

ferences in the reception of the electrical impulses generated by the tag detectors and receiving detectors are a function of the angular displacement of the pendulum wire. The device must be mounted on a structure in such a way that the pendulum wire is located between two straight lines intersecting at the axis of rotation of the reflecting element (mirror), and passing through the first and the second tag detector. Owing to the use of a rotating laser beam, the device allows the continuous measurement of changes to the inclination of a structure relative to the pendulum wire, while the use of an electronic system enables remote, reliable, and above all, precise measurement of these changes. Pendulums controlled by devices with the remote measurement of deviations can be connected to automated control systems of hydro-technical structures.

In the described device, there is no need to define the angle of the emitted laser beam relative to the horizontal, or the angular positioning of the detectors.

In the presented solution, two devices with a rotating laser beam (Fig. 2) are installed at a right angle to determine the pendulum wire displacements in the perpendicular axes  $X$  and  $Y$ . The devices can be adjusted along both  $X$  and  $Y$  axes which have been oriented accordingly to the orientation of  $X$  and  $Y$  axes of coordinate system established on the object for manual measurements.

Taking into account the specificity of different hydro-technical structures and conditions in which they operate, an inductive device was designed, with which measurements of the pendulum wire displacements in conditions of high dustiness and



Fig. 2. Laser devices mounted on a structure

humidity can be performed. Inductive sensors which allow non-contact measuring, searching for the wire, and registering changes to the position of the pendulum wire, were used in this device. Inductive sensors are characterized by trouble-free operation and high resistance to harsh outdoor conditions.

Figure 3 shows examples of operating conditions of devices for measuring the pendulum wire displacements. As can be observed, the operating conditions of automated devices measuring changes to the pendulum wire position are very difficult; they are also difficult to handle by persons performing these measurements manually.



Fig. 3. A measuring position of pendulum wire displacements using a mechanical device

This device consists of a cross-truck and a truck-mounted measuring head with five inductive sensors (Fig. 4). The cross-truck is fixed to a support plate and the whole is encased in a housing, from which the measuring head with inductive sensors juts out. The cross-truck is moved by screws with a pitch of 2 mm, which are rotated by stepper motors with a frequency of 200 steps per revolution. This allows measuring the pendulum wire displacement in the  $X$  and  $Y$  axes with an accuracy of 0.01 mm. In practice, it is estimated that the measurement accuracy of the device should be not less than 0.05 mm with the measuring range of 40 mm.

The measuring head shown in Figure 4 is equipped with five inductive sensors. The coarse sensor is designed to search for the initial pendulum wire position and may be fixed along the  $X$  or  $Y$  axes. In the figure, the sensor is mounted along the  $Y$  axis. After mounting the device on a structure and connecting it to the electronic systems, the device pro-

ceeds to search for the position of the pendulum wire. To accomplish this, the head, together with the table, moves along the  $X$  axis in the entire measuring range, and if the coarse sensor does not register the wire position, the cross-truck with the head moves along the  $Y$  axis within the measuring range of the coarse sensor, and the return shift of the head along the  $X$  axis follows. These activities are carried out until the coarse sensor detects the position of the pendulum wire. Following the lo-

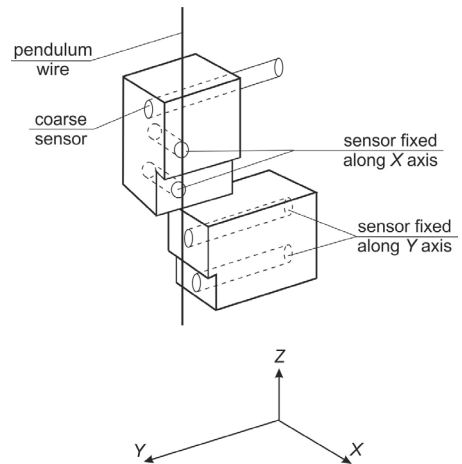


Fig. 4. A diagram of the measuring head

cedure of the wire position by the coarse sensor, a shift of the cross-trucks along the  $X$  and  $Y$  axes occurs so that the wire is recorded by the two sensors mounted along the  $X$  axis, and the two sensors mounted along the  $Y$  axis. Such a shift is possible because the distances between the coarse sensor and the sensors mounted along the  $X$  and  $Y$  axes are known structurally. This shift is implemented by a measuring programme controlling the operation of the stepper motors. From this point, when the wire moves relative to the sensors mounted along the  $X$  and  $Y$  axes, the logical statuses at their output will change, and the stepping motors guiding the measuring head with the sensors mounted along the  $X$  axis and  $Y$  axis will be activated so that the pendulum wire reaches the position at the intersection of the planes passing through the sensors of the  $X$  and  $Y$  axes. In order to determine the direction of the pendulum wire displacement, the fronts of the sensors placed along the  $X$  and  $Y$  axes are shifted

relative to each other. If the  $X$  axis or  $Y$  axis sensors do not send electrical impulses, it means that the wire is moved away from these sensors, and the control systems will run the motors and cause the automatic alignment of the tables with the head by as much as is necessary to have the signal from only one sensor mounted along the  $X$  and  $Y$  axes. However, when signals are received from both of the sensors mounted at the  $X$  or  $Y$  axes, the tables and the head will be moved away, since it means that the pendulum wire is too close to the inductive sensors. Truck sliding tables have predetermined fixed zero positions against which the magnitude of the displacement will be determined. The magnitude of the pendulum wire displacement along the  $X$  and  $Y$  axes will be measured based on counting the steps made by the stepper motors sliding the tables, and thus by the measuring head along the  $X$  and  $Y$  axes.

The cross truck table, stepper motors, and the measuring head (on the left in the figure) of the inductive device for measuring the pendulum wire displacement are shown in Figure 5.



Fig. 5. The inductive device without its housing at a test stand

The use of such instruments for measuring tall buildings, especially hydro-technical structures, will allow a more accurate and easier analysis of their behaviour, and the evaluation of their safety.

### 3. Trial tests

Test stands, on which shifts in the  $X$  and  $Y$  axes within the range of up to 25 mm and with an ac-

curacy of 0.01 mm can be made, were designed and constructed for the laboratory testing of devices designed to measure pendulum wire displacements.

The results of laboratory tests of the device with a rotating laser beam are shown in Table 1, where  $X_s$  and  $Y_s$  are the reference displacements, respectively along the  $X$  and  $Y$  axes, whereas  $X_p$  and  $Y_p$  are the readings of the device for the displacements along the  $X$  and  $Y$  axes, respectively.

The differences  $X_s - X_p$  and  $Y_s - Y_p$  between the reference displacements and the readings of the device in the  $X$  and  $Y$  axes respectively (Table 1) do not exceed 0.02 mm. It also follows from the data presented in Table 1 that the measuring accuracy of the device obtained during the tests should be confirmed in the course of the pendulum wire displacement measurements in the field, at a hydro-technical facility.

Table 1. The results of measuring structure deformations [mm]

No	$X_{\text{man}}$	$X_{\text{las}}$	$X_{\text{man}}(n-1)$	$X_{\text{las}}(n-1)$
1	8.73	0.29	-0.11	-0.09
2	8.62	0.20	-1.24	-1.18
3	7.38	-0.98	-0.10	-0.06
4	7.28	-1.04	-0.03	0.01
5	7.25	-1.03	0.00	0.04
6	7.25	-0.99		

On account of the optical systems used in this solution, the device may be used at structures with average dustiness and humidity. As part of the tests performed, the prototype was mounted and tested at a hydro-technical structure, where the results of the  $X_{\text{las}}$  values of the pendulum wire displacement measured with the device practically did not differ from the  $X_{\text{man}}$  results of measurements made using a manual instrument (Table 2).

Table 1 shows the results of measuring structure deformations which occurred within a period of two months. The maximum difference of readings of the manual and laser instruments was 0.06 mm, and is within the measurement error of the manual instrument.

The results of measurements taken using the manual device are the mean values of several measurements taken.

Table 2. Results of laboratory tests of the device with a rotating laser beam [mm]

No	$X_s$	$Y_s$	$X_p$	$Y_p$	$X_s - X_p$	$Y_s - Y_p$
1	0.000	0.000	-0.004	-0.006	0.004	0.006
2	0.000	5.000	-0.002	4.998	0.002	0.002
3	5.000	5.000	5.015	5.018	-0.015	-0.018
4	-5.000	5.000	-4.993	4.988	-0.007	0.012
5	-5.000	10.000	-4.992	9.994	-0.008	0.006
6	-10.000	5.000	-10.003	4.983	0.003	0.017
7	-10.000	0.000	-9.993	-0.001	-0.007	0.001
8	-10.000	-5.000	-10.015	-5.002	0.015	0.002
9	-10.000	-10.000	-9.997	-10.001	-0.003	0.001
10	0.000	-10.000	-0.010	-10.009	0.010	0.009
11	5.000	-10.000	5.008	-10.011	-0.008	0.011
12	10.000	-10.000	9.984	-9.994	0.016	-0.006
13	10.000	-5.000	9.995	-4.992	0.005	-0.008
14	10.000	0.000	9.998	-0.018	0.002	0.018
15	10.000	5.000	9.998	4.994	0.002	0.006
16	10.000	10.000	10.003	10.003	-0.003	-0.003
17	-10.000	10.000	-10.010	9.986	0.010	0.014
18	0.000	0.000	-0.006	-0.010	0.006	0.010

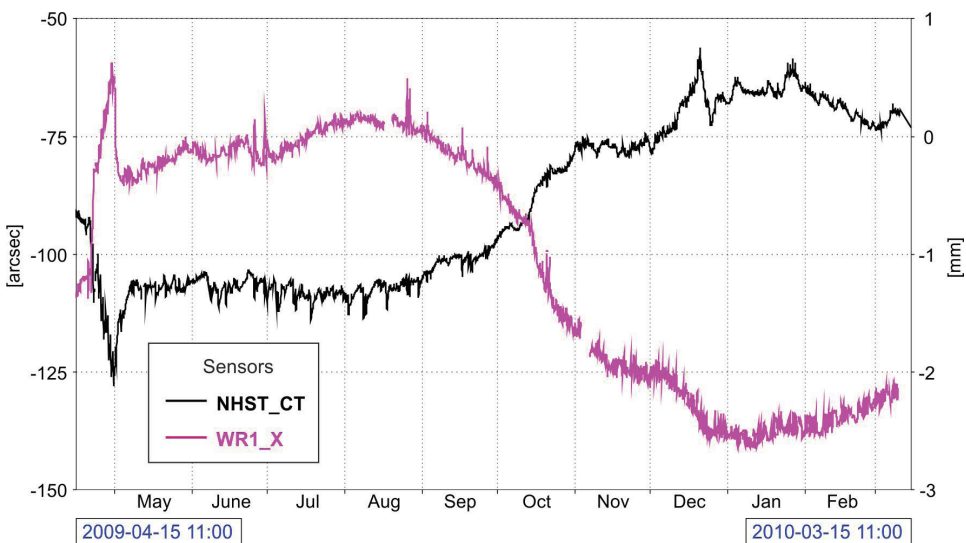


Fig. 6. The results of measurements taken using the laser device at a hydro-technical facility

Table 3. Results of the laboratory tests of the inductive device [mm]

No	$X_s$	$X_p$	$X_p(n-1)$
1	-4.0	1.36	0.49
2	-3.5	1.85	0.52
3	-3.0	2.37	0.53
4	-2.5	2.90	0.48
5	-2.0	3.38	0.47
6	-1.5	3.85	0.49
7	-1.0	4.34	0.53
8	-0.5	4.87	0.48
9	0.0	5.35	0.48
10	0.5	5.83	0.49
11	1.0	6.32	0.53
12	1.5	6.85	0.48
13	2.0	7.33	0.47
14	2.5	7.80	0.50
15	3.0	8.30	0.53
16	3.5	8.83	0.53
17	4.0	9.36	

Table 2 shows the measurement readings only on the  $X$  axis, since changes in the readings on the  $Y$  axis proved insignificant.

Figure 6 shows the measuring results of the laser device for measuring the pendulum wire displacement (violet), performed at a hydro-technical facility over a period of one year. In the first stage of the measurements large deformation of the object can be observed. It was correlated with the complete emptying of the tank and its filling after technical inspection. The variations in the object deformation recorded over the entire measuring campaign reflect the effects of the normal exploitation of the object, i.e. periodic drain water from the water reservoir and then refilling it as a regular. Long periodic sinusoidal deformation is due to seasonal changes of water temperature. The measured structure deformations amounted to about 3 mm. Their nature is similar to the nature of the mirror reflection of changes recorded using a hydrostatic levelling instrument (black). The frame of reference defining the direction of displacements of the laser device was not synchronized with the appropriate frame

of reference of the hydrostatic levelling instrument (Table 2).

The device for measuring the pendulum wire displacements with a rotating laser beam was presented at the IWIS 2010 exhibition of inventions in Warsaw, where it was awarded a medal.

The inductive device for measuring the pendulum wire displacement was also examined at a new test stand of measuring range of 40 mm, and part of these tests was presented in Table 3.

In Table 3,  $X_s$  stands for the reference pendulum wire displacements by 0.5 mm in the range of 8 mm, whereas  $X_p$  stands for the values measured using the inductive device for measuring the pendulum wire displacements.

The difference between successive measurements taken using the inductive device was presented in column  $X_p(n-1)$ .

The differences between the reference readings and those of the inductive device do not exceed plus/minus 0.03 mm, and constitute accuracies sufficient when measuring structure displacements and deformations with the measuring range of 40 mm.

## 4. Conclusions

The results of the laboratory tests and those conducted at the hydro-technical facility clearly indicate that the devices presented can be used for taking measurements in field conditions, and work in the automated measuring system existing in a structure, taking measurements of the pendulum wire displacements at the same time as instruments measuring parameters such as temperature, humidity, water level, the width of expansion joints, inclination, date, time, etc. Simultaneous measurements of all parameters enable a more accurate and faster analysis of correlations between the measured parameters at the controlled structure (Janusz and Janusz, 2005).

## Acknowledgements

Research and design works were carried out as part of the statutory tasks of the Institute of Geodesy and Cartography. Field studies were carried out at a facility belonging to the Directorate of Porąbka-Żar Pumped-Storage Power Plant. The electronics, measurement programmes, and the installation of the device at the facility were developed and performed by the company OLBRYSZ Electronic.

## References

- Brys H., (2000): *The geometry of displacements and deformations of the concrete section of a dam* (in Polish), XV Konferencja katedr i zakładów geodezji na wydziałach niegeodezyjnych, 25–26.09.2000 r.
- Brys H., Cmielewski K., (2004): *A device for determining changes to the bending line of tall engineering structures* (on Polish), uprawniony: Politechnika Krakowska im. Tadeusza Kościuszki, patent nr PL204782 z dnia 13.09.2004.
- Cmielewski K., (2003): *An instrument for measuring changes to the deviations of engineering structures, especially dams* (in Polish), uprawniony: Uniwersytet Przyrodniczy we Wrocławiu, patent nr PL201918 z dnia 19.12.2003.
- Janusz W., Smolka M., Kolodziejczyk M., (1974): *A catalogue of marks and measuring and control devices for measuring structure displacements and deformations* (in Polish), zeszyt B, Instytut Geodezji i Kartografii.
- Janusz J., Janusz W., (2004): *The methodology of testing the susceptibility of water damming structures to load changes* (in Polish), Seria Monograficzna Nr 9, Instytut Geodezji i Kartografii, Warszawa, 85 pp.
- Janusz J., Janusz W., (2005): *Measurements are just the beginning* (in Polish), Geodeta IX 2005 r.
- Kolodziejczyk M., Olbrysz P., (2007): *Laser devices for measuring pendulum wire displacements* (in Polish), uprawniony: Instytut Geodezji i Kartografii, Olbrysz Electronics Spółka Cywilna, patent nr PL210419 z dnia 02.10.2007.
- Mirek G., (2003): *The design of a linear displacement sensor and its use in determining changes to the position of a physical pendulum* (in Polish), XVIII Konferencja katedr i zakładów geodezji na wydziałach niegeodezyjnych, Warszawa - Rogów 4–6.09.2003, pp. 181–188.
- Ohtomo Fumio, (2003): *Photodetection device for rotary laser system*, patent No EP 1 524 498, priority number JP20030353826, priority date 14.10.2003.
- Smolka M., (1994): *A system of remote and automated measuring of displacements and deformations of large structures* (in Polish), Zeszyty Naukowe AR Wrocław, Geodezja i Urządzenia Rolne, z. 251, pp. 75–82.

## Urządzenia do automatycznego pomiaru przemieszczeń drutu wahadła

Mieczysław Kolodziejczyk

Instytut Geodezji i Kartografii, ul. Modzelewskiego 27, 02-679 Warszawa

Tel.: +48 22 3291912, Fax.: +48 22 3291950 E-mail: mieczyslaw.kolodziejczyk@igik.edu.pl

**Streszczenie:** W artykule opisano konstrukcję i zasadę działania dwóch prototypowych urządzeń: urządzenia laserowego i urządzenia indukcyjnego, służących do pomiaru przemieszczeń drutu wahadła. W pierwszym urządzeniu zastosowano wirującą wiązkę laserową oraz dwa detektory wewnętrzne (stałe) i dwa detektory zewnętrzne. Wiązka laserowa padając na detektory powoduje wygenerowanie przez nie sygnałów elektrycznych. Różnice czasowe wygenerowanych sygnałów przez detektory wewnętrzne (stałe) i detektory zewnętrzne są funkcją przemieszczenia drutu wahadła. W drugim urządzeniu zastosowano czujniki indukcyjne zamocowane w głowicy pomiarowej, która jest przytwierdzona do wózka krzyżowego, który przesuwa się wzdłuż prostopadłych do siebie osi  $X$  i  $Y$  w zakresie 50 mm. Wózek jest przesuwany silnikami krokowymi a umieszczone w osiach  $X$  i  $Y$  czujniki indukcyjne wyszukują położenie drutu wahadła. Liczba kroków silników krokowych jest miarą przemieszczenia drutu wahadła wzdłuż osi  $X$  i  $Y$ .

Urządzenia takie są stosowane do kontroli odchyleń od pionu wysokich obiektów hydrotechnicznych głównie na skutek działania naprężeń wewnętrznych i czynników zewnętrznych jak temperatura i poziom wody w zbiorniku.

**Słowa kluczowe:** odchylenie od pionu, pomiar przemieszczeń, wahadło, drut wahadła, objekty hydrotechniczne

# INSTRUCTIONS TO AUTHORS

**GEOINFORMATION ISSUES (Problemy Geoinformacji)** is a journal issued 1-2 times a year, publishing peer-reviewed articles covering theoretical, experimental or applicable problems of geodesy, surveying engineering, photogrammetry, cartography, GIS and remote sensing.

## Legal requirements

The author(s) guarantee(s) that the manuscript will not be published elsewhere in any language without the consent of the copyright owners, that the rights of the third parties will not be violated, and that the publisher will not held legally responsible should there be any claims for compensation.

Authors wishing to include figures or text passages that have already been published elsewhere are required to obtain permission from the copyright owner(s) and to include evidence that such permission has been granted when submitting their papers. Any material received without such evidence will be assumed to originate from the authors.

## Manuscript submission

Submission of the manuscript implies that the work has not been published before (except in form of an abstract or as a part of a published lecture, review or thesis); that it is not under consideration for publication elsewhere; that its publication has been approved by all co-authors, if any, as well as by the responsible authorities at the institution where the work was carried out.

Manuscripts should be submitted in English in electronic form to the Editor-in-Chief of GEOINFORMATION ISSUES, 27 Modzelewskiego St., 02-679 Warsaw, Poland, tel:+48 22 3291904, fax:+48 22 3291950, e-mail: geoinfo@igik.edu.pl. Please be sure to include your e-mail address and your fax as well as phone number. The manuscripts and figures will not be returned, unless specifically requested by the authors.

In case the manuscript has more than one author its submission should include the list specifying contribution of each author to the manuscript with indicating who is the author of the concept, assumptions, research methodology, data processing. Major responsibility is of the author submitting the manuscript.

The Editor will counteract in GEOINFORMATION ISSUES against *Ghostwriting*, i.e. when someone

substantially contributed to the preparation of the manuscript but has neither been included to the list of authors nor his role is mentioned in the acknowledgements as well as *Ghost authorship*, i.e. when the author/co-author did not contribute to the manuscript or his contribution is negligible. Any detected case of *Ghostwriting* and *Ghost authorship* will be exposed and the appropriate subjects, i.e. employers, scientific organisations, associations of editors etc, will be informed.

## Electronic submission of a manuscript

### Layout guidelines:

- use a normal, plain Times Roman font for text, italics for textual emphasis, bold for mathematical vectors,
- use the table functions of your word processing program, not spreadsheets, to make tables,
- use the equation editor of your word processing program for equations,
- place all figures with figure legends and tables with table legends in the manuscript,
- submit also all figures as separate files.

### Data format:

Save your manuscript in RTF or DOC Microsoft Word for Windows format.

### Illustrations:

Figures should be provided in the vector graphics. The preferred figure format is CDR (Corel Draw), XLS (Microsoft Excel), EPS. Exceptionally JPG or TIF (specifically for halftone illustrations) formats will be accepted. The filename should include the figure number. Figure legends should be included in the text and not in the figure file. Scanned line drawings should be digitised with a minimum resolution of 800 dpi relative to the final figure size. For digital halftones, 300 dpi is usually sufficient. Non-standard fonts used in the vector graphics must be included. Please do not draw with hairlines. The minimum line width is 0.2 mm (0.567 pt) relative to the final size.

### Delivery of a manuscript:

Please send your manuscript, preferably a zip file (text and illustrations in separate files, unencoded) either by e-mail or on a CD ROM. Please always supply the following information with your data: operating system, word processing program, drawing program, image processing program, compression program. The file name should be memorable (e.g. author name), have no more than 8 characters, and include no accents or special symbols.

### Manuscript preparation

Manuscripts should be typed in single-line spacing throughout on the A4 sheet with 2.5 cm margins.

#### 1. Title page:

- a concise and informative title,
- the name(s) of the author(s),
- the name(s) and address(es) of the affiliation(s) of the author(s),
- the e-mail address, telephone and fax numbers of the communicating author.

2. **Abstract:** the paper must be preceded by a sufficiently informative abstract presenting the most important results and conclusions.

3. **Keywords:** three to five keywords should be supplied.

4. **Introduction:** should state the purpose of the investigation and give a short review of the pertinent literature.

5. **Acknowledgements:** should be brief and consist of grant or individuals that require acknowledgement. The names of funding organizations or institutions providing data should be given in full.

6. **References:** the list of references should be in alphabetical order and should only include works that are cited in the text and that have been published or accepted for publication. Personal communications could only be mentioned in the text. References should consist of the complete list of authors and should be given in the following form:

– journal articles:

Blais J.A.R., Lodwick G.D., Ferland R., (1983): *Gravimetric terrain corrections in western Canada*, Canadian Journal of Earth Science, Vol. 20, No 2, pp. 259–265.

– books:

Heiskanen W.A., Moritz H., (1967): *Physical geodesy*, W.H. Freeman and Company, San Francisco.

– multi-author books (proceedings):

Rummel R., (2000): *Global unification of height system and GOCE*, in: M.G. Sideris (ed), Gravity, Geoid and Geodynamics 2000, IAG Symposia, Vol. 123, Springer, pp. 13–20.

In the text, references should be cited by author(s) last name and year: e.g. (Beutler, 2003a), (Müller and Rapp, 1993), (Schwarz et al., 1990), (Sjöberg et al., 2000; Sideris, 2001b; 2002).

7. **Formulae and symbols:** must be written legibly and will be typeset in italics. One-layer indexing is preferable. Numbering of formulae, if necessary should be given in brackets fitted to the right margin.

8. **Footnotes:** to the text should be numbered consecutively and placed on the bottom of the page to which they refer. Footnotes to the tables should be indicated by superscript lowercase letters.

9. **Illustrations and tables:** all figures (photographs, graphs or diagrams) and tables should be cited in the text and each numbered consecutively throughout. Lowercase roman letters should identify figure parts. Figure legends must be brief and must contain self-sufficient explanations of the illustrations. Each table should have a title and a legend explaining any abbreviation used in that table.

10. **Units:** SI units must be used.

11. **Running head:** consisting of at most 60 characters a concise banner representing the title of the article must be submitted by the author(s).

### Proofreading

Proofreading is the responsibility of the author. Corrections should be clear; standard correction marks should be used. Corrections that lead to a change in the page layout should be avoided. The author is entitled to formal corrections only. Substantial changes in content, e.g. new results, corrected values, title and authorship are not allowed without the approval of the editor. In such case please contact the Editor-in-chief before returning the proofs.

### Free copy

Each author will receive one complimentary copy of the current journal. All copies are supplied to the communicating author.

---

Cena 25,00 PLN (w tym 5% VAT)

#### Please mail orders and inquiries to:

Institute of Geodesy and Cartography  
27 Modzelewskiego St.  
02-679 Warsaw, Poland  
tel. +48 22 3291918, fax +48 22 3291950  
e-mail: boi@igik.edu.pl

#### Zamówienie krajowe można składać do:

Instytutu Geodezji i Kartografii  
ul. Modzelewskiego 27  
02-679 Warszawa  
tel. +48 22 3291918, fax +48 22 3291950  
e-mail: boi@igik.edu.pl